Quantum Gates Using Majorana Modes in Nanowires

Master's Thesis in Physics

Sebastian Östnell

Department of Physics
University of Gothenburg
Gothenburg, Sweden 2019

Quantum Gates Using Majorana Modes in NanoWires

Sebastian Östnell

Supervisor:
Henrik Johannesson

Examiner:
Mats Granath

January 31, 2019
Department of Physics
University of Gothenburg

Author: Sebastian Östnell

Email:
sebbe.ostnell@hotmail.com

FIM945 - Physics Master Thesis
Supervisor: Henrik Johannesson
Examiner: Mats Granath

Department of Physics
University of Gothemburg
SE-412 96 Göteborg
Sweden
+46 (31) 772 1000

Göteborg, Sweden 2019

Abstract

This thesis explores the use of Majorana modes in nanowires for quantum computations, taking off from a T-junction construction proposed by Alicea et al. (Nat. Phys. 7 (5) (2011) 412-417). The basic theory of Kitaev's chain model is presented, and two single qubit gates are explicitly constructed using the T-junction formalism. The thesis bridges the gap between braiding diagrams and a corresponding physical implementation.

Contents

1

Introduction

Realising a fully functioning quantum computer is sometimes considered as a major threshold to be overcome in order to better understand the universe. Using quantum bits, the promise of the quantum computer lies in having the ability to simulate quantum systems as well as expeditiously solving models of large complex dynamical systems: Anything from weather pattern prediction and medical compound fabrication to simulating the beginning of the universe.

A common problem that has plagued systems intended to be used for quantum computing is their sensitivity to external sources of disturbance, where the qubits (atoms, ions, quantum dots, etc.) of the computational system decohere too fast to be useful. To solve the issue of rapid decoherence, one idea that has surfaced in the last decade is to utilise a well known property of a special particle known as a Majorana fermion. Majorana fermions have been hypothesised to appear as quasiparticles in condensed matter systems under special conditions.

The basic idea can be described as follows: First, it is possible to describe an electron as consisting of two Majoranas. Under a change of basis, the two Majoranas can become spatially separated. The original electron state is then insensitive to external sources of decoherence as any effective perturbation must act on the two separate Majorana states simultaneously. Simply put, the electron state effectively splits into two non-local Majorana states and is therefore protected.

The problem associated with using Majorana fermions for quantum computations is related to creating and manipulating Majoranas in a system supporting large numbers of qubits, the scale of the computing system. This is where the work of Alicea et al. [1] comes into the picture. They show how it would be possible to create and manipulate quasiparticle Majorana modes in a nanowire network consisting of multiple T-junctions units (two connected wires perpendicular to one another). Scaling up the system only requires connecting more identical T-junctions to the network. This wire network allows for the creation, transport, braiding and fusing of Majorana states.

1.1 Purpose and Outline

In this thesis we will explore the nanowire T-junction construction proposed by Alicea et.al [1]. In chapter 2 we lay the groundwork and look at the fundamental properties of the Majorana fermion. In chapter 3 we review the derivation of the proposed nanowire construction, examine the interchange of particles using T-junctions, and discuss how the nanowire network may be used to build quantum gates in chapter 3. We use the nanowire network in chapter 4 to explicitly construct two single qubit gates. Chapter 5 contains a brief summary and an outlook for future work.

2

Theory

The original idea resulting in what we now call a 'Majorana fermion' was originally proposed in a 1937 paper authored by Ettore Majorana [2]. The idea was to show that spin-1/2 particles could be described without resorting to the complex valued fields used in the Dirac equation, and therefore serve as a description of fermionic particles without the need for negative energy states. While the positron had already been discovered in 1932, Majorana motivated the need for a purely real equation describing fermionic particles using symmetry arguments as well as the possibility that it might have been a necessary equation to use for the neutrino and neutron [2]. Majoranas modified Dirac equation describes a spin $\frac{1}{2}$, electrically neutral, fundamental particle. Any fundamental particle that is neutral is also its own antiparticle. An example of an electrically neutral particle which is its own antiparticle is the photon, a bosonic particle.

There also exist electrically neutral fermions like the neutron, a spin-1/2 particle composed of three quarks, and thus, not a fundamental particle. As such, neutrons will not be considered in this thesis.

The seemingly simple switch from complex-valued fields to real-valued fields have large implications for the resulting particle states. While historically relegated to a position of a simple quirky stumbling step on the road towards the standard model, these particles states have been gaining interest from a completely different perspective over the last decade, namely from condensed matter physics.

There are "Majorana-like" states expected to form in condensed matter systems and such states have been shown to exhibit another remarkable feature: the particle exchange statistics governing them is **non-abelian** [3]. Unlike the abelian fermionic and bosonic exchanges, in a non-abelian exchange the order in which it is performed does matter, the elements a and b of a non-abelian group do not commute:

$$(a * b) \neq (b * a). \tag{2.1}$$

The non-abelian nature of the Majorana-like states have made these quasiparticles gain renewed interest from theoretical condensed matter physicists. The principal reason for this lies in the possibility to use the Majorana-like states for quantum computations [4]. We will now introduce the Majorana fermion, Majorana modes and finish with a short introduction to quantum computing.

2.1 Majorana Fermions

The Majorana fermion was for a long time relegated to the annals of history as a mathematically quirky modification to Dirac theory with little use outside of answering the question of physics students "what if the Dirac field were real valued?". Nowadays the question has returned with force. First, the possibility of neutrinoless double beta decay [5, 6] have revived Majorana's hypothesis in the realm of elementary particle physics. Secondly, and more relevant to this thesis, new developments in condensed matter physics, to be reviewed below, have put the Majorana fermion back in the spotlight, brighter than ever.

Before getting into the peculiar nature of Majorana's hypothetical particles, we will briefly review the Dirac equation and its implications. Then we will contrast the Majorana particle with a regular Dirac particle, the electron.

2.1.1 The Dirac Equation

In 1928 Dirac presented a relativistic wave equation suitable for describing electrons [7]. This was a revolutionary paper since it firmly established a proper relativistic quantum theory for spin-1/2 particles.

Previous forays into the field we now call quantum mechanics started at the turn of the previous century. In 1900 Max Planck presented an empirical formula intended to solve the problem of "how does the frequency of light depend on the temperature of the emitter", the black body problem. Max Planck is nowadays famous for stating that "it was an act of despair" that lead to the famous relation:

$$E = h\nu, \tag{2.2}$$

where h is Plank's constant and ν is the frequency of the corresponding emitted light. This was the first important step to the formal quantization of light and earned Planck a Nobel prize in 1918. Albert Einstein famously used Plank's quantization to explain the photoelectric effect in a 1905 paper that subsequently led to Einstein being awarded the Nobel prize in 1921.

Important strides in the budding field of quantum mechanics was later made in the 1920's by Erwin Schrödinger and Werner Heisenberg. Based on the ideas of particle-wave duality from Louis de Broglie and building on the quantization of light by Einstein, Schrödinger's work yielded a non-relativistic wave equation for elementary particles, the Schrödinger equation of non-relativistic quantum mechanics:

$$i\hbar\frac{\partial}{\partial t}\Psi = H\Psi, \tag{2.3}$$

where $H = -\frac{h^2}{2m}\nabla^2 + V$, $\hbar = \frac{h}{2\pi}$, Ψ is the wave function, m is the particle mass, V is an interaction potential, and ∇^2 is the Laplace operator that only acts on the spatial components of Ψ.

The Hamiltonian H is based on the expression for the total energy of a classical system

$$E = \frac{p^2}{2m} + T = H, \tag{2.4}$$

and therefore did not work at all in a relativistic setting. Thus, it was soon realized to be an incomplete, although useful, description of Nature[8].

After the establishment of the Schrödinger equation the next logical step was to find a similar wave equation that accounts for the relativistic energy-momentum relation

$$E^2 - \vec{p}^{\,2}c^2 = m_0^2c^4. \tag{2.5}$$

Here c is the speed of light, m_0 is the rest mass of the particle in question and $\vec{p}^{\,2}$ is the momentum vector. Since we are now looking at a relativistic situation we can express the energy-momentum relation in a covariant way. Assuming a free particle situation for simplicity

$$p^\mu p_\mu - m^2c^2 = 0. \tag{2.6}$$

Here p_μ are components of a four-vector, $\vec{p} = (p_0, p_1, p_2, p_3)$.

Using this relation and following a similar derivation as that of the Schrödinger equation, the relativistic wave equation we call the Klein-Gordon equation end up as:

$$\frac{1}{c^2}\frac{\partial^2}{\partial t^2}\Psi = (\nabla^2 - \frac{m^2c^2}{\hbar})\Psi, \tag{2.7}$$

for a particle with mass m. Note that for this relativistic equation the wave-function Ψ is now a four-component, complex-valued function of time and position in space. The Klein-Gordon equation was actually derived by Schrödinger before the non-relativistic equation named after him. The reason he abandoned it in favour of the non-relativistic version was due to the failure of the Klein-Gordon equation to reproduce the correct energy levels for the Hydrogen atom, since the Klein-Gordon equation does not account for spin. As such the Klein-Gordon equation only works when describing the behaviour of relativistic particles with **zero spin**, for example the Higgs boson. This limits the usefulness of the Klein-Gordon equation in particle physics since the Higgs boson is the only known fundamental particle with spin zero. The stable particles that were under investigation at that time (1920's/ 1930's) were the spin-1/2 proton and the spin-1/2 electron, the latter particle of special interest due to the evolving understanding of atomic structure at that time.

To properly describe quantized relativistic spin-1/2, Dirac worked to find an equation that was consistent with the relativistic energy-momentum relation as well as linear in the time, as the Schrödinger equation is. To start the search, Dirac "factorized" the relativistic energy-momentum relation [cf. eq. (2.6)]:

$$p^\mu p_\mu - m^2c^2 = (A^\kappa p_\kappa + mc)(\gamma^\lambda p_\lambda - mc) = 0. \tag{2.8}$$

Here A^κ and γ^λ are undetermined objects with κ, λ = 0,1,2,3, i.e. together representing a total of eight coefficients. To determine what the objects are, we expand eq. (2.8):

$$(A^\kappa p_\kappa + mc)(\gamma^\lambda p_\lambda - mc) = A^\kappa\gamma^\lambda p_\kappa p_\lambda - mc(A^\kappa - \gamma^\kappa)p_\kappa - m^2c^2 = 0, \tag{2.9}$$

and to avoid terms linear in p_κ we chose that $A^\kappa = \gamma^\gamma\delta_{\gamma\kappa} = \gamma^\kappa$.

$$\gamma^\kappa\gamma^\gamma p_\kappa p_\gamma - mc(\gamma^\kappa - \gamma^\kappa)p_\kappa - m^2c^2 = 0. \tag{2.10}$$

Now we must determine what the γ^κ objects are, conditioned by

$$p^\mu p_\mu = \gamma^\kappa\gamma^\lambda p_\kappa p_\lambda. \tag{2.11}$$

It is at this stage in the investigation Dirac had an inspired idea:, the γ^κ objects are **matrices**, not numbers(!), as one might have thought a first glance. The proper matrices are four-dimensional and generated by the Clifford algebra $Cl_{1,3}(R)$, fulfilling the conditions

$$\{\gamma^\mu, \gamma^\nu\} = 2\eta^{\mu\nu}, \qquad \mu,\, \nu = 0, 1, 2, 3, \tag{2.12}$$

where $\eta^{\mu\nu}$ is the Minkowski metric for flat spacetime. The so called **gamma matrices** can be represented in different ways. In the Dirac basis the matrices are written as:

$$\gamma^0 \doteq \begin{bmatrix} \mathbf{I} & 0 \\ 0 & \mathbf{I} \end{bmatrix} \qquad \gamma^i \doteq \begin{bmatrix} 0 & \sigma^i \\ \sigma^i & 0 \end{bmatrix} \qquad i = 1,2,3. \tag{2.13}$$

Here $\mathbf{I}$ is the 2×2 identity matrix, 0 is the 2×2 null matrix and $\sigma^i, i = 1,2,3$, are the three Pauli matrices. Utilising the gamma matrices, we return to the factorization of the energy-momentum relation (eq. (2.8)):

$$p^\mu p_\mu - m^2c^2 = (\gamma^\kappa p_\kappa + mc)(\gamma^\lambda p_\lambda - mc) = 0, \tag{2.14}$$

and pick out the second factor (by convention) and find the Dirac equation, commonly written in natural units ($\hbar = c = 1$) as:

$$(\gamma^\mu p_\mu - m)\Psi = 0 \qquad \textbf{(Dirac equation).} \tag{2.15}$$

The Dirac field Ψ is a four-component field called a Dirac spinor. These spinors are the correct objects to use when describing electrons in relativistic quantum mechanics. A final comment: for notational simplicity we don't explicitly write out that the mass term of the Dirac equation is implicitly multiplied by a 4×4 identity matrix in spinor space:

$$m = \; m \; \times \mathbf{I}_{spin} = \begin{bmatrix} m & 0 & 0 & 0 \\ 0 & m & 0 & 0 \\ 0 & 0 & m & 0 \\ 0 & 0 & 0 & m \end{bmatrix}. \tag{2.16}$$

2.1.2 Antimatter

We now want to illustrate how the Dirac equation predicts antimatter using a simple example: we will look at the wave function for a free fermion at rest, a plane wave solution with $\vec{p} = 0$ for the Dirac spinor :

$$\Psi(x^\mu) = u(p^0)e^{-ip\cdot x}. \tag{2.17}$$

The Dirac eq. (2.15) now gives us:

$$(\gamma^0 p_0 - m)\Psi = (\gamma^0 E - m)\Psi = 0 \;\; \rightarrow \;\; Eu = \begin{bmatrix} m\mathbf{I} & 0 \\ 0 & -m\mathbf{I} \end{bmatrix} u. \tag{2.18}$$

The solutions to these equations are four eigenspinors:

$$u^1 = \begin{bmatrix} 1 \\ 0 \\ 0 \\ 0 \end{bmatrix} \quad u^2 = \begin{bmatrix} 0 \\ 1 \\ 0 \\ 0 \end{bmatrix} \quad u^3 = \begin{bmatrix} 0 \\ 0 \\ 1 \\ 0 \end{bmatrix} \quad u^4 = \begin{bmatrix} 0 \\ 0 \\ 0 \\ 1 \end{bmatrix}, \tag{2.19}$$

with each an associated fermion wave function

$$\Psi^1 = u^1 e^{-im\cdot t}, \quad \Psi^2 = u^2 e^{-im\cdot t}, \quad \Psi^3 = u^3 e^{+im\cdot t}, \quad \Psi^4 = u^4 e^{+im\cdot t}. \tag{2.20}$$

This give us four solutions instead of the expected two spin projections of a fermion. Note that the four solutions come in two sets of two solution each, where the sign of the plane wave exponents are either $e^{im\cdot t}$ or $e^{-im\cdot t}$. This seems to suggest that Dirac theory produces states with negative energy(!), $E = -m$. How to explain it? Dirac proposed that the vacuum was in fact a "sea" filled with negative energy particles, and as such any particle behaving as a positively charged electron, was actually a "hole" in the Dirac sea. While this explanation for elementary particles eventually fell apart after the positron was discovered in 1932 [9], the notion of a sea of fermions survived in the realm of condensed matters theory (see section 2.1.4).

With the discovery of antimatter in 1932, the negative energy solutions of the Dirac equation were re-examined and nowadays we have reinterpreted them using a simple Bogoliubov transformation that identifies the fermion states with creation and annihilation operators of real physical particles [10]. The creation and annihilation operators associated with the Dirac fermions are written as

$$c_x^\dagger \text{ and } c_x, \tag{2.21}$$

with the subscript $_x$ referring to the specific particle type; electron/ positron/ muon etc. These operators can be seen as either creating or destroying particles in the state $|X\rangle$. They can also be seen as creating particles or antiparticles, both with positive energy ($E > 0$) and both with opposite charges. The fermion creation and annihilation operators act on particle states according to the following rules:

$$\begin{aligned} c^\dagger |0\rangle = |1\rangle, \quad c^\dagger |1\rangle = 0, \\ c |1\rangle = |0\rangle, \quad c |0\rangle = 0. \end{aligned} \tag{2.22}$$

Note that a fermion state cannot contain two or more particles at the same time: the Pauli principle is enforced as a result of the Fermi-Dirac statistics governing the spin-1/2 particle operators:

$$\{c_x^\dagger, c_y^\dagger\} = 0, \quad \{c_x, c_y\} = 0, \quad \{c_x^\dagger, c_y\} = \delta_{xy}. \tag{2.23}$$

2.1.3 Majorana's Modification

Majorana's modification of the Dirac equation [2][11] results in real-valued fields describing electrically neutral spin-1/2 particles called Majorana fermions. The equation is written as

$$(\tilde{\gamma}^\mu p_\mu - m)\tilde{\Psi} = 0. \tag{2.24}$$

To ensure that the fields $\tilde{\Psi}$ are purely real, we must make sure that the $\tilde{\gamma}^\mu$ components are all purely imaginary, in contrast to the γ^μ in the Dirac basis (2.13):

$$\begin{aligned} \tilde{\gamma}^0 &\doteq \begin{bmatrix} 0 & \sigma^2 \\ \sigma^2 & 0 \end{bmatrix}, \qquad \tilde{\gamma}^1 \doteq \begin{bmatrix} i\sigma^1 & 0 \\ 0 & i\sigma^1 \end{bmatrix}, \\ \tilde{\gamma}^2 &\doteq \begin{bmatrix} 0 & \sigma^2 \\ -\sigma^2 & 0 \end{bmatrix}, \qquad \tilde{\gamma}^3 \doteq \begin{bmatrix} i\sigma^3 & 0 \\ 0 & i\sigma^3 \end{bmatrix}. \end{aligned} \tag{2.25}$$

The resulting solution to the Majorana equation 2.24 now fulfills the reality condition

$$\tilde{\Psi} = \tilde{\Psi}^*. \tag{2.26}$$

The corresponding particles, the Majorana fermions, are usually represented by

$$\gamma \text{ and } \gamma^\dagger. \tag{2.27}$$

The corresponding creation and annihilation operators now becomes the one and the same, since complex conjugation of a real-valued operator is the same operator:

$$\gamma = \gamma^\dagger. \tag{2.28}$$

Since the operators are now the same, the singular spin-1/2 particle state that emerges is its own anti-particle state, just like the photon is its own antiparticle. There is no longer any antiparticle states that appears to have negative energy present. This feature alone was the principal "aesthetic reason" for Majorana's decision to create a modified Dirac equation.

As the neutron and neutrinos were eventually understood better in the following years after Majorana's 1937 paper, the modification of the Dirac equation never gained further development until the "Majorana-like" states in condensed matter theory returned the name Majorana to the forefront of physics (see chapter 2.1.5 for a proper introduction).

2.1.4 Majorana Fermions in Nature

Majorana proposed in his 1937 paper that the neutrons and (the still hypothetical at that time) neutrino particles [2] could possibly be accurately described by his equation and therefore be Majorana fermions. We now know that the neutron is in fact a composite particle, composed by three quarks held together by the strong force. As far as neutrinos are concerned the situation is a little different. After the discovery of neutrinos in 1956 [12] it was quickly determined that neutrinos were in fact *not* Majorana fermions since neutrinos and anti-neutrinos are distinctly different particles. This is seen from the conservation of lepton number, where the number of leptons plus the number of antileptons is a conserved quantity in elementary particle physics. Each neutrino species is connected one-to-one with each lepton: electron (e), muon (μ) and tau (τ).

An example of this is the decay of pions, where a positive (negative) pion decays into a muon μ and a muon-neutrino ν_μ (muon-antineutrino $\bar{\nu}_\mu$):

$$\begin{aligned} \pi^+ &\to \mu^+ + \nu_\mu, \\ \pi^- &\to \mu^- + \bar{\nu}_\mu. \end{aligned} \tag{2.29}$$

So far the difference may be only superficial, nothing more than a bookkeeping method used in the standard model. However, the neutrinos produced in the pion decay of equation 2.29 may induce neutron-to-proton conversions and the antineutrinos produced may induce proton-to-neutron conversion given sufficient incident energy:

$$\begin{aligned} \nu_\mu \text{ allows for: } & \nu_\mu + n \to \mu^- + p^+ \quad \text{yet doesn't allow for: } \nu_\mu + p^+ \to \mu^- + n, \\ \bar{\nu}_\mu \text{ allows for: } & \bar{\nu}_\mu + p^+ \to \mu^- + n \quad \text{yet doesn't allow for: } \bar{\nu}_\mu + n \to \mu^- + p^+. \end{aligned} \tag{2.30}$$

This behaviour indicates that the difference between neutrinos and antineutrinos are more than superficial, and thus, if they are distinct particles then are clearly not Majorana fermions.

In the years since their original discovery, observations of neutrino emissions from the sun show that neutrino species oscillate over time and only a "total neutrino number" $L_\tau + L_\mu + L_\sigma$ seems to be conserved [13]. A possible explanation involves a concept known as "sterile neutrinos" [6] that may be fundamental Majorana fermions.

These developments suggest physics beyond the standard model and thus opens up the possibility to reconsider whether the discrepancies between neutrinos and antineutrinos may instead be explained by a neutral neutrino being produced with either a left handed chirality for the $\pi^+ \to \mu^+ + \nu_\mu$ decay and a right handed chirality for the $\pi^- \to \mu^- + \bar{\nu}_\mu$ decay [14].

If the future shows that neutrinos/ antineutrinos are in fact indistinguishable, then Majorana's hypothesis was correct all these years and Majorana fermions are in fact all around us.

An alternative route to finding Majorana fermions in nature is to search the realm of condensed matter systems where new and exotic states of matter arise when a many-particle system is driven into a special phase by an external influence, like an electromagnetic field or a change of temperature. One example of this is the fact that electrons in metals can pair together to form bosonic-like "particle states" capable of forming Bose-Einstein-like condensates. This effect is seen in superconducting states of matter, where electron-phonon interactions overcomes the electrical repulsion between electrons and Cooper pairs form [15]. These are now known as conventional superconductors.

These emergent "particles" that form can only exist in a background system, not as free constructs outside a containing system. They are known as **quasiparticles**, emergent phenomena that can be interpreted and measured as if the background system did contain these quasiparticles as regular particles. Quasiparticles are mathematically treated within the same framework as real observable particles, although the physical understanding of what a particle/ quasiparticle or state represent in reality is different. A particularly simple example is the transport of an electron in a semiconductor: the effective quasiparticle has the same charge as a regular electron but the its mass can be significantly larger. This "heavy electron" is a result of the underlying collective motion of electrons inside the atomic lattice of the conducting material [16].

Another instance where quasiparticles in a condensed matter systems demonstrate a striking similarity to fundamental particles is in the electron-hole state. These hole states share the name that Dirac used to explain the negative energy solutions found in his equation (see section 2.1.2). In Dirac's theory of fundamental physics the negative energy solution was later explained as a positron, discovered in 1932 [9]. Unlike the positron, the hole states in condensed matter theory are explained as the collective effect from an electron that is actually missing from the atom in the material.

The electron and its "anti-particle", the hole state, are described by the same mathematical structure as the electron and the positron, and are understood in the same language of second quantization.

To understand the hole state we need to look at the background system in a typical case. In the atomic lattice of a condensed matter system, the absence of an electron leaves a net positive charge at the location of the hole. To examine the holes closer we now look at the ground state of a condensed matter system. The model we use for the ground state is the zero-temperature electron gas [16]. This is a simple model that accounts for the Fermi-Dirac statistics of an electron (eq. (2.23)).

To describe the multiple electrons in the electron gas we introduce **multiparticle states** [17]. We begin by looking at the vacuum state. The vacuum state has by definition no particles occupying any of the available states and it has the following form in the **occupation number representation**

$$|0\rangle = |0_1, 0_2, 0_3, \,,...\rangle\,. \tag{2.31}$$

In our example we will fill these states with electrons. Due to the Fermi statistics of the electrons, only one electron per site is possible (ignoring spin). In order to find the energy of the ground state of a condensed matter system with N electrons, all electrons must occupy the lowest available single-particle energy states.

To create an electron in a state we use the $c_i^\dagger$ creation operator from eq. (2.21) as follows

$$c_i^\dagger\,|0\rangle = |0_1, 0_2, 0_3, \,,... 1_i, \,..., \,0_N\rangle\,, \tag{2.32}$$

and we use the corresponding c_i annihilation operator to remove the particle

$$c_i\,|0_1, 0_2, 0_3, ..., 1_i, \,..., 0_N\rangle = |0\rangle\,. \tag{2.33}$$

The ground state ("GS") for a system containing N electrons is

$$|GS_e\rangle = |1_1, 1_2, 1_3, ..., 1_N\rangle\,. \tag{2.34}$$

The energy level filled by the last (highest energy) electron is called the **Fermi energy** E_F. If we look at the electron wave functions filling up the ground state [16], we can transform to momentum space through

$$E_F = \frac{\hbar^2 k_F^2}{2m}. \tag{2.35}$$

Through this relation the Fermi energy E_F corresponds to a sphere in k-space (momentum space) with radius k_F (**Fermi wave vector**) [16][18]. Using the Fermi surface we have now a good tool to show how the holes are formed.

In the ground state, the Fermi sphere is completely filled and any new electron states being added must have an energy above E_F and their corresponding position in k-space (k_i) will lie outside k_F [19]. To illustrate the creation and annihilation of particles outside the ground state i.e. electrons with occupation number $i > N$ from eq. (2.34). We will use the "new" operators $a_i^\dagger$ and a_i for this purpose.

When $k_i > k_F$:

$$\begin{aligned} & a_i^\dagger\,|GS_e\rangle \\ &= \; a_i^\dagger\,|1_1, \,..., \,1_N, 0_{N+1}, 0_{N+2}, \,...\rangle \\ &= \quad |1_1, \,..., \,1_N, 0_{N+1}, 0_{N+2}, \,..., \,1_i, \,...\rangle \\ &\rightarrow \;\; a_i^\dagger = c_i^\dagger \;\text{for}\, i > N, \end{aligned} \tag{2.36}$$

and

$$\begin{aligned} a_i \left|1_1, ..., 1_N, 0_{N+1}, 0_{N+2}, ..., 1_i, ...\right\rangle \\ = \left|1_1, ..., 1_N, 0_{N+1}, 0_{N+2}, ..., 0_i, ...\right\rangle \\ = \left|GS_e\right\rangle \\ \rightarrow \quad a_i = c_i \ \text{for}\, i > N. \end{aligned} \tag{2.37}$$

We see that the $a_i^\dagger$/ a_i operators create/ annihilate electrons at higher energy levels (as expected).

Now we look at what happen when we do a similar operation inside the Fermi sphere using the "new" operators $b_i^\dagger$ and b_i. Since the states inside the Fermi sphere are already filled, the added energy cannot create new electrons (Pauli principle) and the result is to excite the electron to a point outside the Fermi sphere, thus removing it from the Fermi sphere.

When $k_i < k_F$:

$$\begin{aligned} b_i^\dagger \left|GS_e\right\rangle = \ & b_i^\dagger \left|1_1, ..., 1_i ..., 1_N,\right\rangle \\ = \ & \left|1_1, ..., 0_i ..., 1_N,\right\rangle \\ \rightarrow \ & b_i^\dagger = c_i \ \text{for}\, i < N. \end{aligned} \tag{2.38}$$

The $b_i^\dagger$ operator has created a hole in the Fermi sphere. Similarly, as the conjugate operator to $b_i^\dagger$, the b_i operator

$$\begin{aligned} b_i \left|1_1, ..., 0_i ..., 1_N,\right\rangle = \left|1_1, ..., 1_i ..., 1_N,\right\rangle \\ = \left|GS_e\right\rangle \\ \rightarrow \quad b_i = c_i^\dagger \ \text{for}\, i < N. \end{aligned} \tag{2.39}$$

The b_i operator has annihilated a hole in the Fermi sphere, effectively creating an electron in its place.

Just like the fundamental electrons and positrons discussed previously, the electrons and hole-states in a condensed matter systems are interchanged by charge conjugation, implemented by taking $c_{k<k_F}$ into $c^\dagger_{k>k_F}$ and vice versa. This results in a transformation of the electron and hole operators a_i and $b_i^\dagger$ into one another. The operator conditions are $c_{k>k_F}$ for an electron operator and $c_{k<k_F}$ for a hole operator.

From this the hole operators must follow the same Fermion algebra as the electron operators (eq. (2.23)):

$$\{b_i^\dagger, b_j^\dagger\} = 0, \qquad \{b_i, b_j\} = 0, \qquad \{b_i^\dagger, b_j\} = \delta_{ij}. \tag{2.40}$$

Note that the hole states in condensed matter theory are not negative energy states since the Fermi sea the holes occupy interacts with the background, so the problem of infinite decay that existed in Diracs original hole hypothesis does not exist here.

As stated previously, electrons can collectively be induced to form quasiparticles. Intriguingly, quasiparticles can be governed by different statistics than the Fermi-Dirac statistics of the underlying electron. It is also possible for the hole states to be part of such quasiparticles, specifically the quasiparticle known as an **exciton** [20].

Excitons are bound states between an electron and a hole state in a solid state system. The exciton is an electrically neutral quasiparticle resulting from the absorption of a photon by the material, dislocating the electron that absorbed it and the resulting hole is then bound to the excited electron. Via excitons, a system can transport energy without transporting charge.

The simplest operator for creating an exciton has the general form [14]:

$$(c_j^\dagger c_k + c_k c_j^\dagger \left|0\right\rangle \ = X_{Ex}^\dagger \left|0\right\rangle \ = \left|Ex\right\rangle . \tag{2.41}$$

for two distinct states j and k. From this example, we now observe that the exciton remains on the exact same form under charge conjugation. As a result the exciton is created and annihilated by the same operator, i.e. the exciton is its own antiparticle.

While the exciton is its own antiparticle, it is a bosonic quasiparticle, in a similar way as a BCS pair in a conventional superconductor, and as such are not Majorana fermions. As it turns out, to find a quasiparticle that fulfills all of the requirements to be a Majorana fermion, we must explore superconducting systems under unusual conditions. As explained previously, in a conventional superconductor the electrons form Cooper pairs that behave as bosons in a Bose-Einstein-like condensate. So while a conventional superconductor is not sufficient to support Majorana fermions, we shall see that it does serve as the basis for producing Majoranas.

2.1.5 Majorana Modes

In the realm of condensed matter physics, quasiparticles like the exciton and the Cooper pair form as effective particles from underlying particle interactions. These interactions can be tuned by controlling internal parameters like crystal structure/ spin-orbit coupling of the material, as well as external parameters like applied electromagnetic fields/ altering the temperature of the system.

One condensed matter system proposed to exhibit Majorana-like states (that from now on we will refer to as Majorana modes) is a system consisting of a nanowire with strong spin-orbit coupling, and deposited on top of a regular superconductor while an incident magnetic field is applied. This is the system discussed by Alicea et al. [1], first proposed independently by [21] and [22]. The setup is shown schematically in Fig. 2.1.

These Majorana modes are quasiparticles inside the nanowire and emerge from the interplay between the induced superconductivity in the wire ("proximity effect" from the regular superconductor) and the spin-orbit coupling, with the interplay controlled by fine-tuning of the applied magnetic field [21, 22].

Let us first look at some features of how we can formally construct Majorana modes out of electrons. The relation between the Majorana modes and the regular electron states from the Dirac equation can be related by a mathematical construction, as one can look at the Majorana state as being "half an electron state", with two real-valued Majorana modes γ_1 and γ_2 combined to form a single complex-valued electron state,

$$\begin{aligned} c_\sigma &= \frac{1}{\sqrt{2}}(\gamma_1 + i\gamma_2), \\ c_\sigma^\dagger &= \frac{1}{\sqrt{2}}(\gamma_1 - i\gamma_2). \end{aligned} \tag{2.42}$$

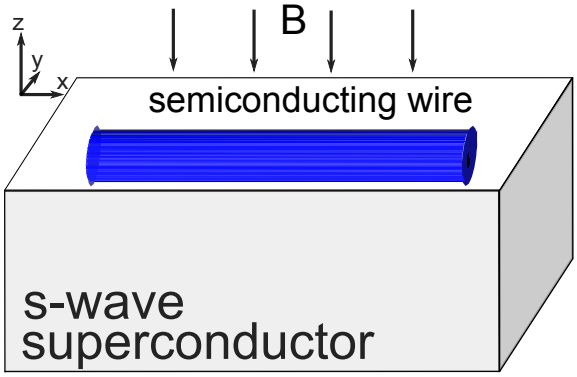

Figure 2.1: A semiconducting wire, deposited on top of a regular superconductor that can be fine-tuned into exhibiting Majorana modes by the application of an external magnetic field.

Here c_σ and $c_\sigma^\dagger$ are the usual electron annihilation- and creation operators, the $_\sigma$ index accounts for spin. The inverse relations are given by

$$\begin{aligned} \gamma_1 &= \frac{1}{\sqrt{2}}(c_\sigma^\dagger + c_\sigma), \\ \gamma_2 &= \frac{i}{\sqrt{2}}(c_\sigma^\dagger - c_\sigma). \end{aligned} \tag{2.43}$$

Here we see that the quasiparticles γ_1 and γ_2 consist of only **one** spin projection. The spin index σ will be omitted in the formulas from this point onward (the single spin index for the Majorana modes contrasts the ordinary Bogoliubov operator for a quasiparticle in an s-wave superconductor which has the form: $b = uc_\uparrow^\dagger + vc_\downarrow$ [23].)

It is easy to verify that the fermion algebra for the c-operators implies that

$$\gamma_k^\dagger \gamma_k \;=\; \gamma_k \gamma_k \;=\; \gamma_k^2 = 1. \tag{2.44}$$

The superconductor imposes an "electron-hole symmetry" on the Majorana modes, relating the creation operator $\gamma_k(E)$ at energy E to the annihilation operator $\gamma_k^\dagger(-E)$ at energy $-E$. Due to this property, the notion of counting the occupancy of Majoranas does not work. A presumed as a Majorana number operator would have the property

$$n_k^M = \gamma_k^\dagger \gamma_k = 1, \tag{2.45}$$

and one concludes that a Majorana mode is in a sense always filled and empty.

Since we can not count if the Majorana states are occupied or not, but we still need to be able to use some form of number states for our eventual physical system we will use the original electrons. As the electrons are regular fermions the number states satisfy

$$\begin{aligned} &\hat{n}_i \left| n_1\, n_2 \ldots n_N \right\rangle \\ =\; &n_i \left| n_1\, n_2 \ldots n_N \right\rangle, \end{aligned} \tag{2.46}$$

where $\hat{n}_i = c_i^\dagger c_i$, $n_i = 0{,}1$.

The Majorana modes described above are purely mathematical constructs, any electron could in principle be decomposed into Majorana modes. The reason this mathematical construction is of any interest is due to the fact that these Majorana modes can actually be detected in the proposed system. An in-depth derivation of the Majorana modes and their physical interpretation follows in chapter 2.2.2.

It is important to note that these Majorana modes are in fact *not* fermions!. They have inherited Majorana's name for the fact that they are self self-conjugate states described by a real Hamiltonian (see section 2.1.3). The actual statistics governing the exchange of two Majorana modes is neither fermionic nor bosonic, instead it is Non-abelian in nature [cf. eq. (2.1)]

An investigation into this feature of the Majorana modes follows. When particle exchange occurs in ordinary particle systems, the resulting change to the wave function is dependent on the particle's **exchange statistics**.

To illustrate the effect of interchanging two particles in a multiparticle state we will be using the exchange operator E_{xc}, with the result

$$\mathbf{E}_{xc}\,|f_1 f_2 ...\rangle = -\,|f_2 f_1 ...\rangle\,, \tag{2.47}$$

in the case of two fermions f_1, f_2 ("π exchange"), and

$$\mathbf{E}_{xc}\,|b_1 b_2 ...\rangle = \;\;|b_2 b_1 ...\rangle\,, \tag{2.48}$$

in the case of two bosons b_1, b_2 ("2π exchange").

For the Majorana modes, there exist **two** distinct exchange operations, clockwise and counterclockwise exchanges, not simply π or 2π exchanges. These **rotations** are implemented by the following operators:

$$\mathbf{E}^{+}_{i,j} \quad \text{and} \quad \mathbf{E}^{-}_{i,j}. \tag{2.49}$$

Leijnse and Flensberg [23] use the work of Ivanov [24] to illustrate the exchange of two Majorana modes isolated in vortices in a 2D $\mathrm{p}_x \pm i\mathrm{p}_y$ superconductor. p-wave superconductivity (spin triplet pairing) is produced when electrons with angular momentum $l = 1$ form Copper-like pairs and condense. The spherical harmonics of the electron pairs in a 2D $\mathrm{p}_x \pm i\mathrm{p}_y$ are [25]:

$$Y_{1,\pm 1} \propto x \pm iy. \tag{2.50}$$

Hence the name $\mathrm{p}_x \pm i\mathrm{p}_y$ superconductor.

The $\mathrm{p}_x \pm i\mathrm{p}_y$ superconductor under consideration by Leijnse and Flensberg [23] consists of a two-dimensional superconductor with triplet pairing and two vortices that host a Majorana mode each. This setup is illustrated in Fig. 2.2. The vortices are associated with a winding of the superconducting phase ϕ by 2π. With a configuration of this sort we can for the sake of simplicity chose to condense the 2π rotation of ϕ around each vortex into a single line where the phase jumps by 2π. By doing so we note that the superconducting phase is single-valued everywhere in the plane except at the so called **branch cut** (the line connected to each vortex). We are free to chose the direction of a branch cut as long as it remains fixed under any Majorana exchanges. The branch cuts are shown as red dotted lines in Fig 2.2.

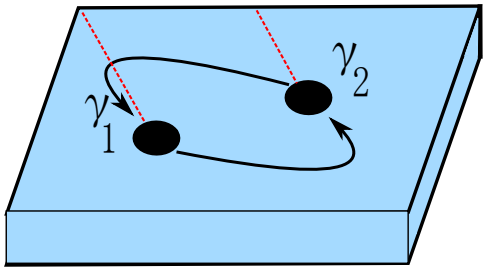

(a) Counterclockwise exchange of γ_1 and γ_2. The vortex containing γ_2 inevitably crosses the branch cut of γ_1.

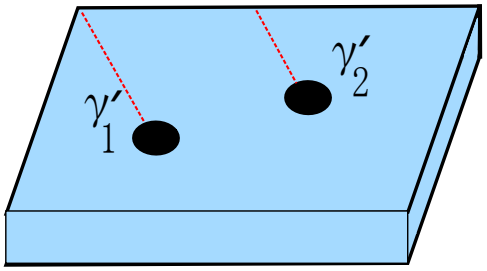

(b) The configuration after the counterclockwise exchange of vortices.

Figure 2.2: Illustration of counterclockwise exchange of vortices in a 2D $\mathrm{p}_x \pm i\mathrm{p}_y$ superconductor. At the branch cut the superconducting phase changes by 2π discontinuously.

Since the superconducting phase is the phase for the electron pairs in the superconductor and since the Majorana modes contained within each vortex are only made up from a single (rather than products of two) fermion operators (eq. (2.42)) [23]. As such, they only acquire a π shift from passing the branch cut.

If we now use the counterclockwise rotation to exchange Majorana γ_1 and γ_2, illustrated in Fig. 2.2:

$$\mathbf{E}_{1,2}^{-} |\gamma_1\gamma_2\rangle \;\rightarrow\; |\gamma_1'\gamma_2'\rangle \,. \tag{2.51}$$

In the basis we have chosen (branch cut orientation), the Majorana modes become

$$\begin{aligned} \gamma_1' &= -\gamma_2, \\ \gamma_2' &= \;\;\gamma_1. \end{aligned} \tag{2.52}$$

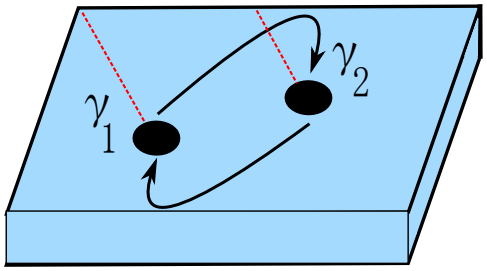

(a) Counterclockwise exchange of γ_1 and γ_2. Here the vortex containing γ_1 inevitably crosses the branch cut of γ_2.

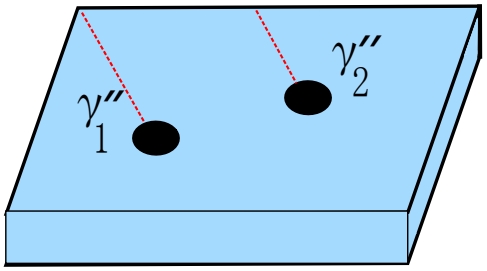

(b) The configuration after the clockwise exchange of vortices.

Figure 2.3: Illustration of clockwise exchange of vortices in a 2D $\mathrm{p}_x \pm i\mathrm{p}_y$ superconductor. At the branch cut the superconducting phase changes by 2π discontinuously.

Then a clockwise rotation in the same system, seen in Fig. 2.3:

$$\mathbf{E}_{1,2}^{+} |\gamma_1\gamma_2\rangle \;\rightarrow\; |\gamma_1''\gamma_2''\rangle \,, \tag{2.53}$$

results in

$$\begin{aligned} \gamma_1'' &= \gamma_2, \\ \gamma_2'' &= -\gamma_1. \end{aligned} \tag{2.54}$$

This property leads us to the non-abelian nature of the Majorana mode exchange, namely that successive exchanges of Majoranas, $\gamma_1 \leftrightarrow \gamma_2$ and $\gamma_2 \leftrightarrow \gamma_3$, do not commute:

$$[\mathbf{E}^+_{1,2}\,,\,\mathbf{E}^+_{2,3}] = \mathbf{E}^+_{1,3}. \tag{2.55}$$

This is unlike the bosonic and fermionic exchanges where the statistics is abelian and the exchanges do commute.

2.2 Kitaev's Chain Model

The model used in this thesis to describe Majorana modes originating from electrons is named after its creator Alexei Kitaev [26]. The purpose of the model was to find the simplest condensed matter system possible where Majorana modes can be induced and actually be detected. As these modes are quasiparticles in a condensed matter system, they are not the fundamental particles Ettore Majorana was describing in his original work, they are in fact the Majorana modes of the preceding chapter (2.1.5).

2.2.1 Electrons to Majorana Modes

To begin looking at the model Kitaev proposed, we will start by describing a one-dimensional system, consisting of a chain of atomic orbitals with electrons allowed to hop from one orbit to its neighbor.

Figure 2.4: N orbitals defining the one-dimensional lattice of the Kitaev model.

Calling the system one-dimensional may seem like we are discussing a hypothetical infinitely thin wire that only exists as an abstract notion. While such a concern could certainly be valid since we are consider generating Majorana modes in a real condensed matter system, we need not worry since the Kitaev model was constructed with nanowires in mind [26]. As the diameters of nanowires are on the order of nanometers (hence the name), the wire has only a few atoms in width while the length of the wire is typically a few hundred nanometers or more, spanning at least a few thousand atoms. Note that as a result of the large length-to-width ratio and since the electron states[1] along the wire are all close to the surface of the wire, no bulk states are available for the electrons to occupy. This is different from a regular 3D materials where almost all electron states are in the bulk.

[1] In the original work by Jason Alicea et al. the electron states originating in the Kitaev chain model, are referred to as "regular fermion states". I chose to refer to these states as "electron states" to anchor the reader to the experimental reality of the actual states in the actual nanowire one would use in practice.

This leads us to Kitaev's proposal where the nanowire system is thought of as consisting of a chain of atomic orbitals, seen schematically i Fig 2.4. In an ordinary tight-binding electron model each site could be occupied by two electrons with different spin projections, "spin up" and "spin down". However, in Kitaev's model we ignore spin, thus we consider a spinless system. As a result of the system being spinless, we only need to consider at most one electron at each physical site (atomic orbital), as follows from the Pauli exclusion principle. We will call these sites either filled or unfilled and describe them mathematically as states in the system as follows:

$$\begin{aligned} \text{Unfilled electron site}: \ |0\rangle\,, \\ \text{Filled electron site}: \ |1\rangle\,. \end{aligned} \tag{2.56}$$

Here the empty state $|0\rangle$ is filled by acting with an electron creation operator, with the same electron creation operator destroying the filled state (Pauli principle). Similarly, the regular electron annihilation operator empties a filled state and destroys an empty state. In formulas:

$$\begin{aligned} c^\dagger\,|0\rangle = |1\rangle\,, \qquad c^\dagger\,|1\rangle = 0, \\ c\ |1\rangle = |0\rangle\,, \qquad c\ |0\rangle = 0. \end{aligned} \tag{2.57}$$

Using this formalism, a fully filled chain of size N is then described as the fully filled electron multi-particle state:

$$|1_1\ 1_2\ 1_3\ ...\ 1_{N-1}\ 1_N\rangle\,. \tag{2.58}$$

Here the index identifying the site number will be particularly relevant when we introduce the Majorana modes later.

The next step is to find Majorana modes in this simple system. To that end we make the observation that the Majorana modes have a peculiar behaviour when combined as in eq. (2.42). From this equation we realise that in fact any electron can be decomposed into a linear combination of Majorana modes.

In any ordinary system containing electrons this observation gives us nothing more than a mathematically correct (but uninteresting) description without any physical relevance, as it amounts to nothing more than a mere change of basis for the electron states.

While this basis change could hypothetically be used as a starting point for further investigations into the possibility that the electron is in fact a composite particle, no free electron would demonstrate this theoretical structure unless the underlying Majorana fermions could be probed individually. Probing the Majoranas individually is not possible in standard model physics as the electron is described as a point-like particle. No experiment on free electrons have hinted at any possible electron substructure.

Yet Kitaev formally introduces two Majorana operators, enumerated by the index j, called c_{2j-1} and c_{2j}, as follows [26]:

$$\gamma_{2j-1} = c_j + c_j^\dagger, \qquad \gamma_{2j} = i(c_j^\dagger - c_j), \qquad j = 1, 2, 3, ..., N. \tag{2.59}$$

$$\gamma_k^\dagger = \gamma_k, \qquad \gamma_k\,\gamma_l + \gamma_l\,\gamma_k = 2\delta_{k,l} \qquad k,\, l = 1, ..., 2N. \tag{2.60}$$

Inverting the relation of eq. (2.59) we find the linear combinations of Majorana operators from which we can construct the original electron operators from:

$$\begin{aligned} c_j &= \frac{1}{2}(\gamma_{2j-1} + i\gamma_{2j}), \\ c_j^\dagger &= \frac{1}{2}(\gamma_{2j-1} - i\gamma_{2j}), \\ j &= 1, 2, 3, ..., N. \end{aligned} \tag{2.61}$$

Note how the index $_j$ relates the quasiparticle Majorana modes to their original electron operators.

In the special case where we have only one electron site in the chain ($N = 1$), we recover the formalism used in chapter 2.1.5 as the relations reduce to:

$$\gamma_1 = c_1 + c_1^\dagger, \qquad \gamma_2 = i(c_1^\dagger - c_1). \tag{2.62}$$

$$\gamma_k^\dagger = \gamma_k, \qquad \gamma_k\,\gamma_l + \gamma_l\,\gamma_k = 2\delta_{kl} \qquad k,\, l = 1, 2. \tag{2.63}$$

$$c_1 = \frac{1}{2}(\gamma_1 + i\gamma_2), \quad c_1^\dagger = \frac{1}{2}(\gamma_1 - i\gamma_2), \quad x = 1. \tag{2.64}$$

2.2.2 Kitaev's Hamiltonian

With the formalism introduced we also note that in any Hamiltonian describing electron dynamics, no term can contain a **single** Majorana mode since that term would not preserve the fermion parity the system inherits from the underlying electrons.

Note that the underlying symmetries of the system follows from the original electrons, since all we have done so far amounts to a change of basis for the system. As a result, the simplest term containing the newly introduced Majorana operators has to be quadratic in $\gamma_{k,l}$.

So the basic model to use for Kitaev's Hamiltonian has to be a simple quadratic Hamiltonian of the form:

$$H = \frac{i}{4}\sum_{k,l} A_{kl}\,\gamma_k\,\gamma_l. \tag{2.65}$$

Here the A_{kl} terms are are limited by hermeticity to be:

$$A_{kl}^* = A_{kl} = -A_{lk}. \tag{2.66}$$

This Hamiltonian gives the correct type of structure to describe the pairing of Majorana operators as required by the fermion parity conservation [26]. To create the correct Hamiltonian for the chain that also exhibits the Majorana modes we want to find, the Hamiltonian must fulfill three conditions.

Firstly, the Hamiltonian must be on quadratic form as explained previously.

Secondly, the typical electron $U(1)$ symmetry: $c_j \rightarrow e^{-i\phi}c_j$, also known as the gauge symmetry of the electric charge (charge conservation), has to be reduced to a Z_2 symmetry: $c_j \rightarrow -c_j$. This is necessary since the Majorana modes created from the electrons in the

chain can't be allowed to mix under any symmetry transformations of the system. If the Majorana modes could be transformed into one another then the system could not be used to transport or braid the Majorana modes and therefore it would be unusable for quantum computations. From this requirement we are lead to consider superconducting system. The specifics of the superconductivity is of no relevance in this case, as long as the electrons form Cooper pairs and break down the $U(1)$ symmetry into a Z_2 electron-hole symmetry. A simple way of visualising the coupling to a superconducting system is to imagine the nanowire (electron chain) deposited on top of a regular superconductor, enabling Cooper pairs to tunnel into the nanowire ("proximity effect").

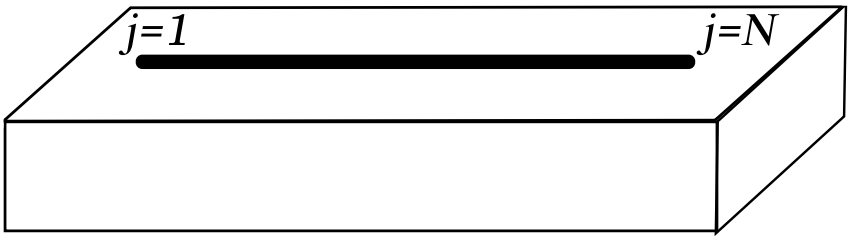

Figure 2.5: A nanowire deposited on top of a superconductor.

Thirdly, the electrons in the chain can not exhibit any spin dependence, "spin up"/ "down", due to the Majorana mode's "electron-hole symmetry", cf. eq. (2.43).

Thus, in this model we will assume that only one spin direction is present. A simple way to achieve this would be to ensure that the nanowire is deposited on top of a p-wave (spin-triplet) superconductor, instead of a regular s-wave superconductor. However, p-wave superconductors are not as readily available as regular s-wave superconductors, therefore we would like to achieve the p-wave pairing using other means. As it turns out, the p-wave pairing can be achieved by the application of a magnetic field on top of the nanowire/ s-wave superconductor construct (for details, see [3]).

Fulfilling these three requirements, the resulting Hamiltonian is called the **Kitaev chain model**:

$$H = -\mu \sum_{j=1}^{N} c_j^\dagger c_j - \sum_{j=1}^{N-1} [t c_j^\dagger c_{j+1} + t c_{j+1}^\dagger c_j + |\Delta| e^{i\phi} c_j c_{j+1} + |\Delta| e^{-i\phi} c_{j+1}^\dagger c_j^\dagger]. \tag{2.67}$$

Here the chemical potential of the electrons are represented by μ. The t-terms describe the effect of a hopping potential (electron motion in the chain), and $|\Delta| e^{i\phi}$ represents the superconducting order parameter induced by the superconductor, with $|\Delta|$ the magnitude of the superconducting gap (roughly the energy to break a Cooper pair) and ϕ a phase picked out spontaneously in the phase-coherent superconducting state [1].

Note that the hopping potential and the induced superconducting pairing connects neighbouring electrons (and their Majorana components), while the chemical potential term counts the electrons present in the system. Remember that each site in the chain can either be occupied by a **single** electron or it can be empty.

To see that Kitaev's Hamiltonian behaves as expected we will first look at the simplest special case, when the chain is undisturbed by the hopping potential and superconducting pairing.

For the trivial case $\mu > 0$ and $t = |\Delta| = 0$:

$$H = -\mu \sum_{j=1}^{N} c_j^\dagger c_j. \tag{2.68}$$

The ground state of the chain is the expected one, with energy $-\mu N_0$, where N_0 is the number of electrons.

If we now shift to the Majorana basis using the appropriate expression, eq. (2.59), and then simplify using (eqs. (2.44), (2.60) and (2.61)), the Hamiltonian takes the form

$$\begin{aligned} H = & -\mu \sum_{j=1}^{N} \frac{1}{\sqrt{2}}(\gamma_{2j-1} - i\gamma_{2j}) \frac{1}{\sqrt{2}}(\gamma_{2j-1} + i\gamma_{2j}) \\ = & -\frac{\mu}{2} \sum_{j=1}^{N} (i\gamma_{2j-1}\gamma_{2j} - i\gamma_{2j}\gamma_{2j-1} + 2). \end{aligned} \tag{2.69}$$

Here we have carried out the multiplication in the new basis and used the Majorana identity $\gamma^2 = 1$ from eq. (2.60). The next step is to do the rewriting

$$\begin{aligned} & -\frac{\mu}{2} \sum_{j=1}^{N} (i\gamma_{2j-1}\gamma_{2j} - i\gamma_{2j}\gamma_{2j-1} + 2) \\ = & -\mu \sum_{j=1}^{N} (i\gamma_{2j-1}\gamma_{2j} + 1) \end{aligned} \tag{2.70}$$

using the anti-commutation relation governing the Majoranas.

Nothing new is gained here, the shift in basis to expose the underlying Majorana modes is just that, a change of basis. This description will however be interesting in the next example, where we will see that the chain can be induced to produce **spatially separated** Majorana modes. The hidden feature of this Hamiltonian which makes this possible is easiest to see for a special case, namely when $\mu = 0$ and $t = |\Delta|$. This choice gives us:

$$H = -t \sum_{j=1}^{N-1} [c_j^\dagger c_{j+1} + c_{j+1}^\dagger c_j + e^{i\phi} c_j c_{j+1} + e^{-i\phi} c_{j+1}^\dagger c_j^\dagger]. \tag{2.71}$$

Now we express this Hamiltonian in the basis of the Majorana operators, just as we did in the preceding example. Note that this time the Majorana operators are differently normalized and they include the superconducting phase term $e^{i\phi}$ from eq. (2.67):

$$\begin{aligned} c_j &= \frac{1}{2} e^{-i\frac{\phi}{2}} (\gamma_{2j} + i\gamma_{2j-1}), \\ c_j^\dagger &= \frac{1}{2} e^{i\frac{\phi}{2}} (\gamma_{2j} - i\gamma_{2j-1}). \end{aligned} \tag{2.72}$$

Inserting these expressions into eq. (2.71):

$$\begin{aligned} H = & -t \sum_{j=1}^{N-1} \left[c_j^\dagger c_{j+1} + c_{j+1}^\dagger c_j + e^{i\phi} c_j c_{j+1} + e^{-i\phi} c_{j+1}^\dagger c_j^\dagger \right] = ... \\ = & -it \sum_{j=1}^{N-1} \gamma_{2j} \gamma_{2(j+1)-1}. \end{aligned} \tag{2.73}$$

The full derivation is simple but somewhat tedious and can be found in the appendix, eq. (A.1).

The final result shows that two Majorana states originating from *different* electrons in the chain pair up and form a new electron state, annihilated by the operator

$$d_j = \frac{1}{2} \left(\gamma_{2j} + i\gamma_{2(j+1)-1} \right). \tag{2.74}$$

As illustrated below for a chain with $N = 4$:

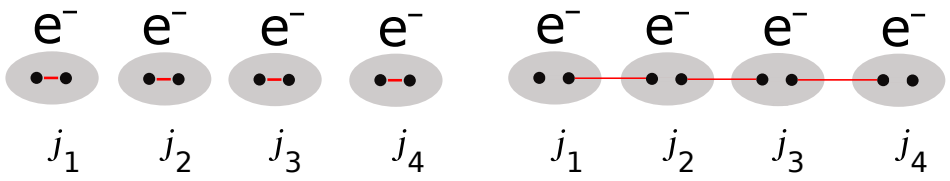

(a) Electrons with Majorana components visible.

(b) Electrons with Majorana components in the shifted basis.

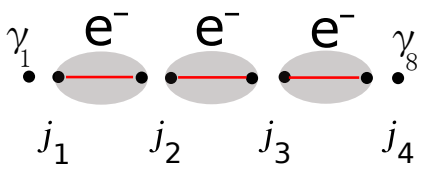

(c) New electrons with edge-Majorana components uncoupled.

Figure 2.6: Majorana component shifting.

Reading from the Hamiltonian in eq. (2.73), we see that the new states cost $2t$ to form. We also see that now the Majorana states sum up to one less state than the corresponding sum in eq. (2.69). The uncoupled, "left over" edge-states must bind together as the Majorana modes cannot exist freely since they represents one half of an electron spin [26]. This forms a non-local electron state that is annihilated by the operator

$$d_{end} = \frac{1}{2} \left(\gamma_1 + i\gamma_{2n} \right). \tag{2.75}$$

Here the two Majorana modes missing from the Hamiltonian in eq. (2.73) are the first and last Majorana modes in the original chain, the edge states. As this state is not present in the Hamiltonian it does not cost any energy to occupy.

It follows that we have a Hamiltonian with two ground states, one empty and one filled with the zero-energy delocalized electron:

$$\begin{aligned} &|0\rangle\,, \\ d_{end}^{\dagger}\,&|0\rangle = |1\rangle\,. \end{aligned} \tag{2.76}$$

As as a result, these two ground states can be used as orthogonal qubit basis states. Note that in this superconducting system we can have an **odd** number of quasiparticles unlike ordinary superconductors where the ground state consists of a superposition of an even number of particle states, forming the Cooper pairs.

2.3 Majorana braiding

Once Majorana modes are created, there are two things we can do to them, **fuse** two Majorana modes or **braid** two Majorana modes.

Since the Majorana states in the nanowires originated from fermion states, one can reform these states by joining the Majorana modes together, thereby fusing them. To braid Majorana modes around each other is to exchange the Majorana modes in either a clockwise or counterclockwise manner. The effects of these braids are shown in section 4.1.

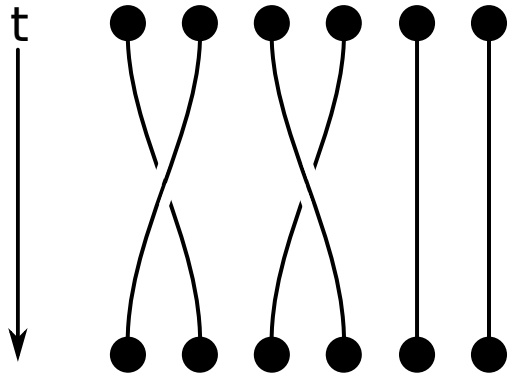

Figure 2.7: A simple braid diagram showing a clockwise braid, a counter clockwise braid and one unperturbed pair.

One can also perform simple translations of the Majorana modes without braiding them, leaving the modes themselves unaffected.

2.4 Quantum Computing

Quantum computing is in essence the quantum analogue of classical computing, where **quantum bits** are operated upon by **quantum gates** to perform calculations [27]. In contrast to classical bits of ordinary computing, quantum bits (abbreviated to **qubits**) are not limited to being in either of two possible states. Instead, a single qubit consists of a superposition of two orthogonal states $|\hat{0}\rangle$ and $|\hat{1}\rangle$.

$$\begin{aligned} &\text{Classical bit: } b = |\hat{0}\rangle \quad \textbf{or} \quad b = |\hat{1}\rangle, \\ &\text{Quantum bit: } Q = c_1|\hat{0}\rangle + c_2|\hat{1}\rangle, \quad |c_1| + |c_2| = 1, \\ &\text{Vector representation: } |\hat{0}\rangle \hat{=} \begin{bmatrix} 1 \\ 0 \end{bmatrix} \text{ and } |\hat{1}\rangle \hat{=} \begin{bmatrix} 0 \\ 1 \end{bmatrix}. \end{aligned} \tag{2.77}$$

In this example the $|\hat{0}\rangle$ and $|\hat{1}\rangle$ states are the **computational basis states** for a single qubit. In a system of **n** qubits there are 2^n mutually orthogonal basis states; as an illustration we look at a three qubit example:

$$\text{Basis states for } \mathbf{n}{=}3 \text{ qubits}: \ |\hat{0}\hat{0}\hat{0}\rangle \ |\hat{0}\hat{0}\hat{1}\rangle \ |\hat{0}\hat{1}\hat{0}\rangle \ |\hat{0}\hat{1}\hat{1}\rangle \ |\hat{1}\hat{0}\hat{0}\rangle \ |\hat{1}\hat{0}\hat{1}\rangle \ |\hat{1}\hat{1}0\rangle \, |\hat{1}\hat{1}\hat{1}\rangle \, . \tag{2.78}$$

To perform calculations we must operate on the qubit states with **quantum gates**. These quantum gates perform a fixed unitary operation on selected qubits. One example is the Pauli X-gate, a single-qubit gate that flips the state it is applied to [28] (it is also possible to construct multi-qubit gates that act on multiple qubits at once).

In the computational basis the Pauli X-gate has the same representation as the Pauli matrix σ_x:

$$\mathbf{X} \hat{=} \begin{bmatrix} 0 & 1 \\ 1 & 0 \end{bmatrix}, \tag{2.79}$$

or, in bra-ket notation:

$$\mathbf{X} \hat{=} |\hat{0}\rangle\langle\hat{1}| + |\hat{1}\rangle\langle\hat{0}|. \tag{2.80}$$

When the Pauli X-gate is applied to the basis states, it flips them:

$$\begin{aligned} \mathbf{X}|\hat{0}\rangle &= \begin{bmatrix} 0 & 1 \\ 1 & 0 \end{bmatrix} \begin{bmatrix} 1 \\ 0 \end{bmatrix} = \begin{bmatrix} 0 \\ 1 \end{bmatrix} = |\hat{1}\rangle, \\ \mathbf{X}|\hat{1}\rangle &= \begin{bmatrix} 0 & 1 \\ 1 & 0 \end{bmatrix} \begin{bmatrix} 0 \\ 1 \end{bmatrix} = \begin{bmatrix} 1 \\ 0 \end{bmatrix} = |\hat{0}\rangle. \end{aligned} \tag{2.81}$$

We formally describe this process as the $|\hat{0}\rangle$ state was transformed into the $|\hat{1}\rangle$ state when we applied the Pauli X-gate to it.

Another quantum gate is the Hadamard gate

$$\begin{aligned} H &\hat{=} \frac{1}{\sqrt{2}} \begin{bmatrix} 1 & 1 \\ 1 & -1 \end{bmatrix}, \\ H &\hat{=} \frac{1}{\sqrt{2}} \Big((|\hat{0}\rangle + |\hat{1}\rangle)\langle\hat{0}| + (|\hat{0}\rangle - |\hat{1}\rangle)\langle\hat{1}| \Big). \end{aligned} \tag{2.82}$$

It is often used as the initial step in a quantum computation since it maps n qubits $|\hat{0}\rangle$ into a superposition of all $2n$ orthogonal states in the computational basis with equal weight and this allows one to one to evaluate 2^n inputs in parallel [28].

The Pauli X-gate and the Hadamard gate will be explicitly constructed by braiding Majorana modes in chapter 4.2.

2.4.1 Universal Quantum Gate

In classical computing there exists two **universal logic gates**. They are known as the NOR (the combination of a NOT and OR gate) and NAND (the combination of a NOT and AND gate). Either one of the two gates can be exclusively used to form all other possible logic gates of classical computing and allow us to perform all classical computations using this single type of gate. The universal gate in quantum computing fills the same role where the repeated use of this quantum gate on different combinations of qubits can generate the action of any other quantum gate.

Since all evolution in a quantum system is unitary, in order for a quantum gate to be universal it is sufficient to be able to generate all unitary transformations of any qubit [28]. There are in fact many combinations of quantum gates capable of fulfilling this requirement [29]. One of these combinations consists of the Hadamard gate, a CNOT (Controlled NOT gate) and any phase gate [28][30]. A common phase gate favoured by condensed matter physicists is the $\pi/8$ gate [1][31].

3

Model Background

In a 2010 paper [1], Jason Alicea et al. presented a design of a nanowire device expected to support Majorana fermion states and allow for the braiding of these states. The proposed construction consists of a series of semiconducting nanowires, deposited on top of a regular s-wave superconductor, where the wires are laid out in a grid of rectangular shapes. The fundamental model Alicea et al. used for their proposed construction is known as the Kitaev Chain Model (explored in section 2.2).

In this model, the network of nanowires placed upon a conventional superconductor can be induced to generate a degenerate ground state in a region of the wires, via a magnetic field. When the system exhibits the degenerate ground state, it allows a new basis to form for the electrons in the wires. In this new basis, the electrons are effectively split apart into non-abelian Majorana modes, (see chapter 2.2.2). The majority of the Majorana states in the topologically non-trivial region form into new electron states, while at each edge of the topological segment there is one Majorana mode "left over" and these two spatially separated Majoranas states form a highly non-local electron state, (see fig. 2.6).

As the distinct segments of the wires are either driven into topologically non-trivial phases or are left unaffected, they create topological and regular regions in the wires. At the interfaces between the topological and non-topological regions, Majorana states form as described by the Kitaev chain model.

The basic components that would allow for the braiding of Majorana states, and as such the usability of the Majorana states for quantum computing, are the T-junctions that form when two wires intersect perpendicularly.

3.1 The Nanowire Construct

The theoretical construction under consideration consists of a series of idealized semiconducting nanowires placed upon an regular s-wave superconductor and subject to a external magnetic field. This condition allows for the formation of topological regions in the wires. At the edges of these regions, Majorana modes form and these Majorana modes can be transported along the wires by the simple application of local voltage gates. Figure 3.1 shows a schematic representation of a single segment of a of nanowire.

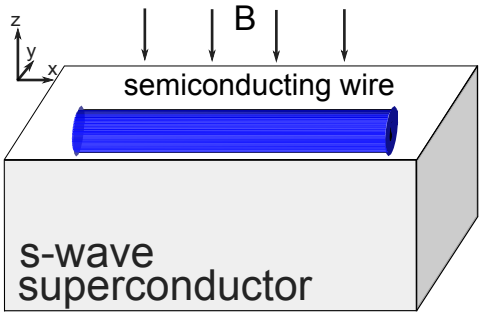

Figure 3.1: A picture of a wire that can be driven into a topological state exhibiting Majorana modes by the application of an external magnetic field.

The basic theoretical description of this wire follows from the work of Alexei Kitaev [26] for which the basics was presented in chapter 2.2.2.

The Hamiltonian used to describe the chain of spinless (p-wave) electrons in the nanowire was derived in chapter 2.2.2 as the Kitaev chain model, eq. (2.67); here we introduce it again to be used as the basis to describe the nanowire construction:

$$H = -\mu \sum_{j=1}^{N} c_j^\dagger c_j - \sum_{j=1}^{N-1} [t c_j^\dagger c_{j+1} + t c_{j+1}^\dagger c_j + |\Delta| e^{i\phi} c_j c_{j+1} + |\Delta| e^{-i\phi} c_{j+1}^\dagger c_j^\dagger]. \tag{3.1}$$

Here the first sum counts the electron states in the chain with μ a chemical potential, and the second sum accounts for the kinetic and interaction energies of the electrons. The terms containing the parameter t describe the tunneling from one site in the chain to the next with the tunneling strength t, this term is also known as the "hopping potential". The parameter $|\Delta| e^{i\phi}$ represents the pairing potential induced by the superconductor that the wire (Kitaev chain) is deposited on top of, where $|\Delta|$ is the superconducting gap and $e^{i\phi}$ is the superconducting phase of the Cooper pairs inherited from the underlying superconductor.

As this Hamiltonian describes the electron behaviour of the idealized nanowire (Kitaev chain), the one thing we can do to produce the Majorana modes we are looking for is to adjust the chemical potential, the tunneling strength and/or the pairing potential. We will follow the blueprint for generating Majorana modes from section 2.2.2. Setting $\mu = 0$, $|\Delta| = t$ gives us the Hamiltonian on the form:

$$H = -t \sum_{j=1}^{N-1} [c_j^\dagger c_{j+1} + c_{j+1}^\dagger c_j + e^{i\phi} c_j c_{j+1} + e^{-i\phi} c_{j+1}^\dagger c_j^\dagger]. \tag{3.2}$$

Expressing the electron operators in terms of Majorana operators [cf. eq. (2.72)]:

$$\begin{aligned} c_j &= \frac{1}{2} e^{-i\frac{\phi}{2}} (\gamma_{2j} + i\gamma_{2j-1}), \\ c_j^\dagger &= \frac{1}{2} e^{i\frac{\phi}{2}} (\gamma_{2j} - i\gamma_{2j-1}). \end{aligned} \tag{3.3}$$

This shift in basis enables us to explicitly see the Majorana modes in the Hamiltonian and how the Hamiltonian under the $\mu = 0$, $|\Delta| = t$ conditions couple together Majorana modes originating from different electrons:

$$-it\sum_{j=1}^{N-1}\gamma_{2j}\gamma_{2(j+1)-1}. \tag{3.4}$$

We will call the states annihilated by

$$d_j = \frac{1}{2}\left(\gamma_{2j} + i\gamma_{2(j+1)-1}\right), \tag{3.5}$$

"new electron states". The change of basis and the formation of new electron states is visualized in the figure below:

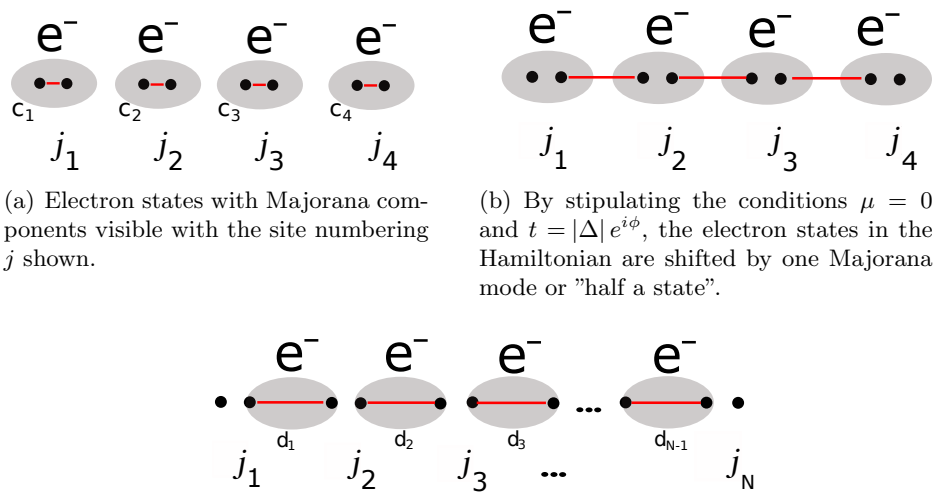

(a) Electron states with Majorana components visible with the site numbering j shown.

(b) By stipulating the conditions $\mu = 0$ and $t = |\Delta|\, e^{i\phi}$, the electron states in the Hamiltonian are shifted by one Majorana mode or "half a state".

(c) The full chain of shifted electron states under the $\mu = 0$ and $t = |\Delta|\, e^{i\phi}$ condition.

Figure 3.2: Electron states in the Kitaev model, before and after the shift of basis.

The special feature of relevance for quantum computations is a special zero-energy state, formed by the Majorana modes missing from eq. (3.4), namely

$$\gamma_1 \quad \text{and} \quad \gamma_{2n}. \tag{3.6}$$

Needless to say, the shift in basis, by which one is looking at the Majorana modes directly instead of looking at the electron states in the Kitaev chain (nanowire), does not affect the original electron states in the wire.

No electron state is missing from the wire, so where has the two missing Majorana components gone? Since they can't have disappeared and also can not exist as free states to conserve the spin of the original electron states, they must form a particle state, specifically a special electron state. This state is annihilated by

$$d_{end} = \frac{1}{2}\left(\gamma_1 + i\gamma_{2n}\right), \tag{3.7}$$

and since it is missing from the Hamiltonian eq. (3.4), the energy cost of occupying this state must be zero! This means we have two ground states $|0\rangle$ and $|1\rangle$ with the property:

$$\begin{aligned} d_{end}^{\dagger}|0\rangle &= |1\rangle\,, \\ d_{end}|0\rangle &= 0. \end{aligned} \tag{3.8}$$

We locate the Majorana *end states* from eq. (3.6) in the chain as follows:

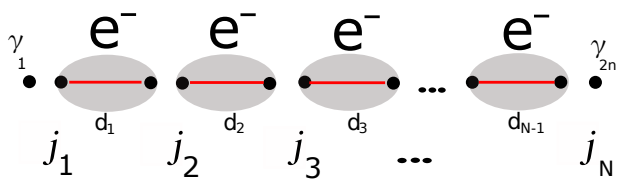

Figure 3.3: The full chain with the end Majorana modes specified as these form the non-local electron state annihilated by d_{end}.

The modes missing from the Hamiltonian, γ_1 and γ_{2n}, with the first Majorana mode originating from the first original electron and the second Majorana mode originating from the last electron as seen in fig. 3.3, must form a highly non-local electron state in the chain.

We can now consider the chain of "new electron states" to be but a small region over a longer Kitaev chain. The region defined by the $\mu = 0$ and $t = |\Delta|$ conditions is called a *topologically non-trivial* region, or a **topological region** for short, as this region which allows for the formation of the Majorana end modes exhibits a different topology than a regular wire. The zero-energy end state from eq. (3.8) is effectively one electron split into two pieces that are separated by a large distance and is therefore difficult to perturb by a local perturbation, (photons/ phonons etc.). This is the case since any potential disturbance of the nanowire must affect both Majorana modes at the same time, else the delocalized electron will be unaffected. This feature is the reason for the ability of the Majorana modes to resist external noise.

3.1.1 A Possible Nanowire

Having looked at the Kitaev system in the previous section, we now turn to the question how to induce a wire to form the topological regions with the desired Majorana modes at the edges. The Kitaev-chain system requires the electrons in the wire to admit only one spin projection (only one pair of Fermi points) as well as forming superconducting p-wave pairs at the Fermi energy. Alicea et al. [1] presents a candidate system which satisfies these conditions: a spin-orbit coupled semiconducting nanowire on top of an s-wave superconductor, with a magnetic field applied perpendicularly [cf. fig. (3.1)]. This nanowire construction and the energy requirements for the formation of Majorana modes was initially investigated by two groups, Lutchyn et al. [21] and Oreg et al. [22].

The simplest Hamiltonian useful to describe such a wire under the required conditions must account for the electron energy, the spin-orbit coupling of the wire, the Zeeman coupling from the magnetic field, and finally the spin-singlet pairing in the wire inherited from the underlying s-wave superconductor via tunnelling of Cooper pairs [32]. We also note that when we now consider a real nanowire in the long-wave length limit we transition into a continuous model, $c_j \to \Psi_x$.

A Hamiltonian that fulfils these prerequisites is the following:

$$H = \int dx \left[\Psi_x^\dagger \left(-\frac{\hbar^2 \partial_x^2}{2m} - \mu - (i\hbar u \hat{e} \cdot \boldsymbol{\sigma} \partial_x) - \frac{g\mu_B B_z}{2}\sigma_z \right) \Psi_x \right. \\ \left. + \left(|\Delta| e^{i\phi} \Psi_{x\uparrow} \Psi_{x\downarrow} + |\Delta| e^{-i\phi} \Psi_{x\uparrow}^\dagger \Psi_{x\downarrow}^\dagger \right) \right], \tag{3.9}$$

where m is the effective electron mass, μ is the chemical potential, u represents the spin-orbit coupling strength, $\boldsymbol{\sigma} = (\sigma_x, \sigma_y, \sigma_z)$ is a vector of Pauli matrices and $\hat{e}$ is the unit vector which the spin-orbit coupling favours to align along or against (we assume in figure 3.1 that $\hat{e}$ lies in the **x,y** plane). We assume also that the magnetic field B_z is perpendicular to the wire. In fig. 3.2 this field is aligned along the z-axis, as seen in the Zeeman-coupling term in eq. (3.9). The last two terms represent the singlet (p-wave) pairing originating from the underlying s-wave superconductor, with the superconducting band gap $|\Delta|$ and superconducting phase ϕ.

To understand the behaviour of this Hamiltonian and how to generate topological regions from the Kitaev Hamiltonian (eq. (3.1)), we will illustrate two special cases, one without the magnetic field ($B_z = 0$) or superconducting gap $|\Delta| = 0$, a second one with the magnetic field tuned to permit the Majorana modes to form.

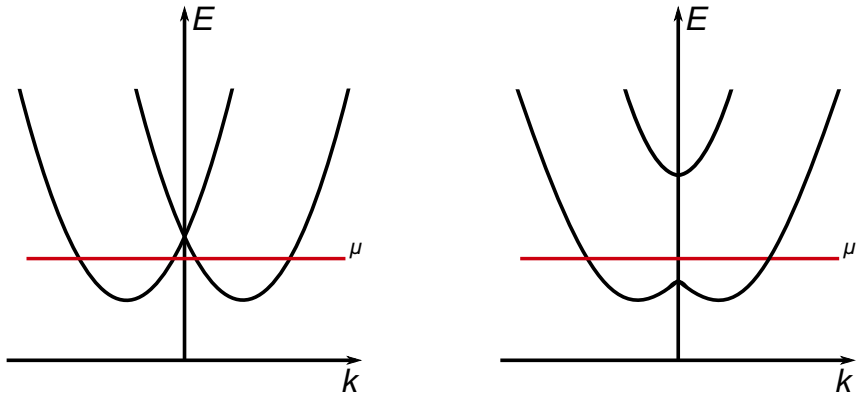

(a) Band structure with $B_z = 0$, no spinless regime, 4 Fermi points.

(b) Band structure with $B_z \neq 0$, implying an effective spinless regime, 2 Fermi points.

Figure 3.4: Band structure of the proposed idealized semiconducting nanowire.

With no magnetic field and hence no band gap, there is no possibility of a spinless region in the nanowire since any value of the chemical potential will result in more than two Fermi points.

Applying the magnetic field B_z generates a band gap at zero momentum ($k = 0$), as seen in fig. 3.4b. When the chemical potential for the electrons in the wire μ lies in this gap the system exhibits a single pair of Fermi points as required. Turning on $|\Delta|$ weakly compared to the gap then effectively p-wave pairs the electrons in the lower band with momentum k and $-k$, driving the wire into Kitaev's topological phase, allowing for the presence of Majorana end modes. The singlet pairing in eq. (3.9) now generates a p-wave pairing since the spin-orbit coupling favours opposite spins for k and $-k$ states. This is so since the locking of spin

to momentum makes spin a superfluous degree of freedom and thus, the electrons in the lower band in fig. 3.4 b) behaves as effectively spinless fermions. This property, coming from the concerted action of the spin-orbit interaction and the applied transverse magnetic field, is what enables p-wave pairing.

It follows that a requirement that has to be fulfilled in order to generate Kitaev's topological phase for a segment of the wire is that

$$|\Delta| < \frac{g\mu_B|B_z|}{2}. \tag{3.10}$$

If the superconducting gap becomes larger than the band gap from the Zeeman effect, the electron pairing will mix states from both the upper and lower bands, violating the "spinless" requirement. The result would be a regular s-wave superconducting segment of the wire without any Majorana modes.

When the wire segment is in the topological phase we can look at yet another special case that illuminates the connection between the wire equation (3.9) and the Kitaev equation (3.1). In the limit where

$$\begin{aligned} mu^2 &\ll g\mu_B|B_z|\,, \\ |\Delta| &\ll g\mu_B|B_z|\,, \end{aligned} \tag{3.11}$$

is fulfilled, the spins of the electrons are nearly completely polarized. This is seen if we use the polarization of the spins to project eq. (3.9) to an equation for a single-band problem, here taken as the lower band from fig. (3.4). Using that the direction of the spin-orbit field ($\sim \hat{e}$) lies in the $x-y$ plane, it is convenient to rewrite the electron operators $\Psi_{x\uparrow}$ and $\Psi_{x\downarrow}$ as

$$\begin{aligned} \Psi_{x\uparrow} &\rightarrow \left(\frac{u(e_y + ie_x)}{g\mu_B|B_z|}\right)\partial_x\,\Psi_x, \\ \Psi_{x\downarrow} &\rightarrow \Psi_x. \end{aligned} \tag{3.12}$$

This allows us to recast eq. (3.9) as an effective Hamiltonian. To leading order:

$$\begin{aligned} H_{\text{eff}} \sim \int dx \Bigg[\Psi_x^\dagger \left(-\frac{\hbar^2\partial_x^2}{2m} - \mu_{\text{eff}}\right)\Psi_x + \\ + \left(|\Delta_{\text{eff}}|\, e^{i\phi_{\text{eff}}}\,\Psi_{x\uparrow}\,\partial_x\,\Psi_{x\downarrow} + |\Delta_{\text{eff}}|\, e^{-i\phi_{\text{eff}}}\,\Psi_{x\uparrow}^\dagger\,\partial_x\,\Psi_{x\downarrow}^\dagger\right)\Bigg], \end{aligned} \tag{3.13}$$

where the modified chemical potential is

$$\mu_{\text{eff}} = \mu + \frac{g\mu_B|B_z|}{2}, \tag{3.14}$$

and the p-wave pairing field is given by:

$$|\Delta_{\text{eff}}|\, e^{i\phi\text{eff}} \approx \frac{\mu|\Delta|}{g\mu_B|B_z|} e^{i\phi}(e_y + ie_x). \tag{3.15}$$

In eq. (3.12) we used that the spin-orbit coupling term ($\hat{e}$) lies in the x, y plane. The key insight gained from this low-energy projected version of the Kitaev Hamiltonian is the directional dependence of the effective superconducting phase. This will be of central importance when we look at networks made up of these wires, see section 3.2.

3.1.2 Majorana Transport in the Wire

Now that we have created Majorana modes at the edges of topological segments, as described in the previous section, the question becomes how to transport them. To answer this question, let us consider the effect of applying a gate voltage.

If we apply a uniform gate voltage over the entire nanowire (resulting in a chemical potential μ as seen in fig. 3.4), the band gap obtained from eq. (3.9) at $k = 0$ then depends on μ as follows:

$$E_{gap}(k=0) = \left| \frac{g\mu_B|B_z|}{2} - \sqrt{|\Delta|^2 + \mu^2} \right|. \tag{3.16}$$

From this we see that the bulk gap closes for a critical value of μ:

$$\mu_c = \sqrt{\left(\frac{g\mu_B|B_z|}{2}\right)^2 - |\Delta|^2}. \tag{3.17}$$

Here we have that $|\mu| < \mu_c$ forms a topological region where Majorana modes emerges while for $|\mu| > \mu_c$ the wire segment is in a topologically trivial phase. This can be visualized by looking at whether μ lies is in the gapped region seen in fig. 3.4(b) as it is in the gapped region the degenerate ground state forms in the wire from the pairing inherited from the proximate superconductor (see fig. 3.1).

When $|\mu| = \mu_c$ the gap closes and new quasiparticles can form or fuse into a regular electron state. This must of course be avoided if we are to transport and braid the Majorana modes without destroying the topological region or creating new topological regions during the transport.

The key to solving this problem with the wire is to use the idea proposed by Alicea et al. [1], namely to use a so called "keyboard" of voltage gates, that can be used to change the voltage over a small localized region of the nanowire. In doing so, the topological region will (locally) expand or contract, moving the Majorana mode at that end of the region in the process. For an illustration, see fig. 3.5:

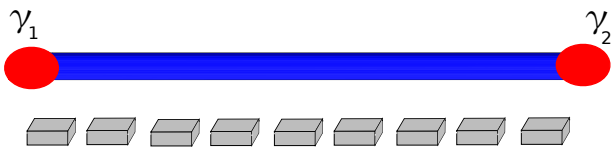

(a) Majorana modes visible in a topological region.

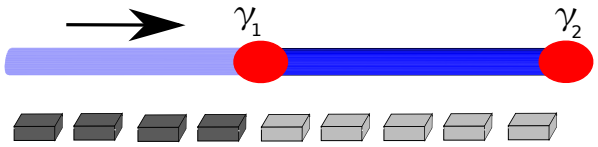

(b) Majorana mode transported by shrinking the topological region using the local voltage gates.

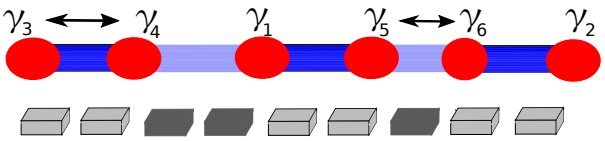

(c) New topological regions formed by using the local voltage gates.

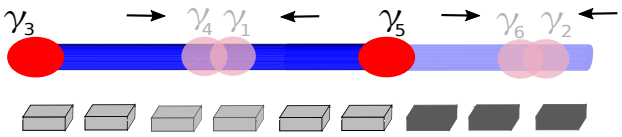

(d) Topological regions fused together using the local voltage gates.

Figure 3.5: A Majorana "keyboard" design, usable for the creation and manipulation of topological regions with their associated Majorana modes.

From figure 3.5 we note that each topological region exhibits two Majorana modes, with one mode at each of its edges. By creating $2n$ Majorana modes in the wire, we gain access to n zero-energy states that expand the number of ground states available to use to store quantum information.

3.1.3 T-junction

We now have a method to create and control Majorana modes in a nanowire. The next step is to braid these to be able to perform quantum computations. Using a single nanowire is not enough since moving the Majorana modes back and forth will only result in meaningless translations or the fusing of Majorana modes, [cf. fig. (3.5)].

The simplest extension to the single nanowire is to use two nanowires that come together to form a T-junction. In this construction it is possible to transport two Majorana around each other and as such we are capable of exchanging Majorana modes using wires.

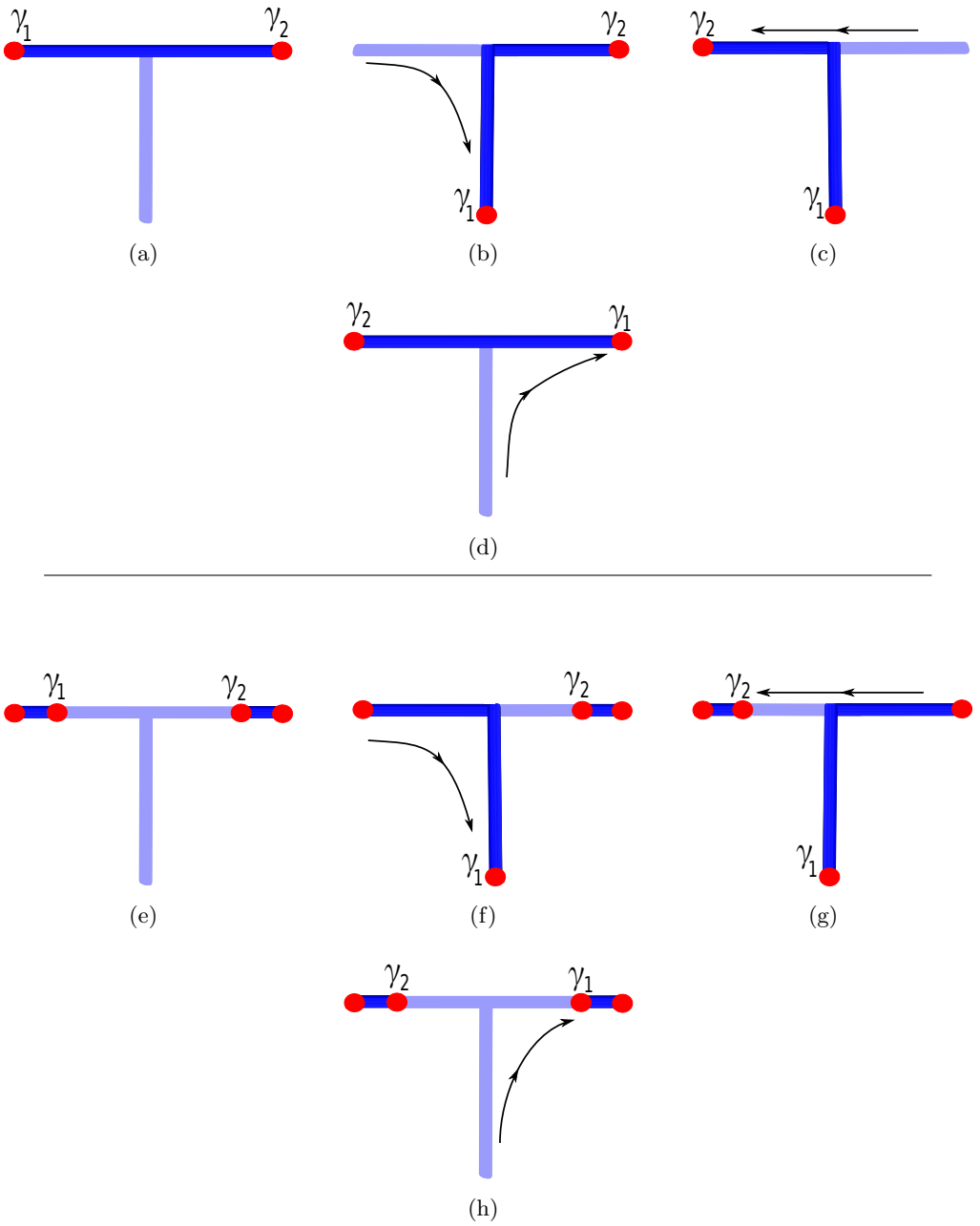

Figure 3.6: Majorana mode transport in a nanowire T-junction, Majorana modes originating from the *same* topological region (a)-(d) and Majorana modes originating from *different* topological regions (e)-(h).

This T-junction construct is the key concept that Alicea et al. invented in their 2010 paper [1].

3.2 Braiding in a Network

At this point we come to the question of how to perform the braiding operations that we would use for quantum computations. To find an answer to that question it is vital that we take a closer look at the T-junction itself.

3.2.1 T-junction Closeup

We begin by making the trivial observation that the T-junction can be seen as an intersection of **three** distinct wire segments, witch we shall call A, B and C respectively. Each segment will be associated with a unique superconducting phase $\phi_{A,B,C}$ inherited from the underlying superconductor, as visualised in fig. 3.8.

There exists a redundancy in the description of the superconducting phase from the underlying model. As described in section 2.2.1, each atomic orbital in the nanowire is associated with an electron site in the chain used to model the nanowire. Each site may be filled by an electron using the $c_j^\dagger$ creation operator. The sites can be labelled from 1 to N in two ways, left to right or right to left.

(a) Left to right. (b) Right to left.

Figure 3.7: Two equally valid ways to label the sites in the chain.

The two choices are equivalent for the chain up to an overall phase for the pair potential term ($|\Delta| e^{i\phi} c_j c_{j+1}$) in eq. (3.1).

After making an initial choice of counting direction, the compensating change that follows from switching the direction of increasing $_j$ is then:

$$|\Delta| e^{i\phi} c_j c_{j+1} \rightarrow |\Delta| e^{i(\phi+\pi)} c_{j+1} c_j. \tag{3.18}$$

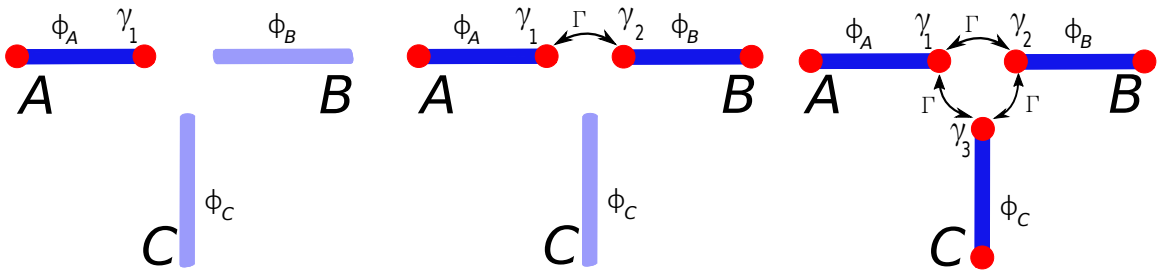

(a) When only a single wire segment contains a Majorana mode no meaningful interaction for that Majorana mode is possible.

(b) With two topological segments there exists a tunneling interaction between the two Majorana modes.

(c) Here all three segments is in a topological phase with three resulting tunneling interactions.

Figure 3.8: Three distinct wire segments in three different topological configurations. Each wire segment has its own topological phase inherited from the underlying superconductor.

One can therefore refer to the phase ϕ in the "left to right" direction while at the same time use the $\phi + \pi$ phase in the "right to left" direction in the same wire segments.

The initial choice of direction must always be specified in order for the wires in a system to be analysed correctly. In this thesis we use the "left to right" convention for horizontal wires and we will use the corresponding "bottom to top" convention for vertical wires, unless otherwise specified.

After the separation of the junction into three wire segments we let the segments interact via single electron tunneling and as such explore the T-junction properties. This is visualized in figure 3.8.

When only one nanowire segment is in a topological phase, only a single Majorana mode is present at the junction, see fig. 3.8a. No tunneling is possible for the Majorana mode in this case, since any single electron interaction is assumed to be small compared to the bulk gap in the wires, similar to the assumptions in section 3.1.1 to ensure that the topological state is confined to the chosen wire segment. While the wave function of Majorana mode γ_1 could in principle be quantitatively affected by the presence of the other wire segments (B and C) through some hypothetical interaction, it is still topologically protected and remain at zero energy. Therefore any such quantitative change is irrelevant to the Majorana mode itself and we now move on to fig. 3.8b.

To understand what happens when two topological segments meet at the junction, as seen in fig. 3.8b, we need to look at the coupling between the Majorana modes. The coupling between the Majorana mode γ_1 at site N of wire A and γ_2 at site 1 of wire B can be characterized by the following Hamiltonian [26],[22]:

$$H_{12} \propto -i\Gamma \cos\left(\frac{\phi_A - \phi_B}{2}\right)\gamma_1\gamma_2. \tag{3.19}$$

This can be understood from eq. (3.3) given that the single-electron tunneling Γ couples the underlying electron states from which the Majorana modes originate. In fig. 3.8b we see that the Majorana modes can remain uncoupled if their respective superconducting phases differ by a factor of π, i.e if the Majorana modes form a so-called **π-junction**. As such no Majorana modes are expected to exist here due to the Majorana-Majorana interaction. The two "potential" Majorana modes should fuse into a regular fermion state as the γ_1 and γ_2 only remain zero-energy modes when the wires form a π-junction ($\phi_A = \phi_B + \pi$). The fusion of Majorana states is illustrated in fig. 3.5d.

Now that we know that the Majorana modes can remain uncoupled in the wires as long as they form π-junctions, we see that we must avoid the nanowire system to form spontaneous π-junctions. For any construction of wires and their corresponding superconducting phase, spontaneous π-junctions would allow a new unwanted Majorana pair to form, in a similar fashion to the formation of Majorana modes seen in fig. 3.5c.

Similar considerations gives us the approximate Hamiltonian describing the final configuration of the T-junction, fig. 3.8c, when all three intersecting wires are in the topological phase:

$$H_{123} \propto -i\Gamma\left[\cos\left(\frac{\phi_A - \phi_B}{2}\right)\gamma_1\gamma_2 + \cos\left(\frac{\phi_C - \phi_B}{2}\right)\gamma_3\gamma_2 + \sin\left(\frac{\phi_A - \phi_C}{2}\right)\gamma_1\gamma_3\right]. \tag{3.20}$$

Here the sine term in the A and C coupling is a consequence off the "left to right" and "bottom to top" conventions, resulting in Majorana mode γ_1 and γ_3 both residing on the

final ("c_N") site in their respective chains. It follows that the coupling is then proportional to $\cos\left(\frac{\phi_A-\phi_C-\pi}{2}\right)\gamma_1\gamma_3 = \sin\left(\frac{\phi_A-\phi_C}{2}\right)\gamma_1\gamma_3$. Note that in this case the requirement for a π-junction is $\phi_A = \phi_C$.

In the three-wire case seen in fig. 3.8c, the expected result of the three Majorana mode interactions (away from the fine-tuned case) is a single Majorana mode remaining with the other two fusing into a regular electron state. The specifics of this fusion is determined by the specifics of the wire segments and their superconducting phase differences. The "surviving" Majorana mode is identified as the one missing from the Hamiltonian in eq. (3.20). This Majorana mode may be either one of the original Majorana modes: γ_1, γ_2, γ_3 or a linear combination of them, whichever is missing from the Hamiltonian.

To illustrate a possible scenario we use the example provided by Alicea et al. [1] where we chose $\phi_A \neq \phi_C$ and $\phi_B = \phi_A + \pi$:

$$H_{123} \propto -i\Gamma \left[\cos\left(\frac{\phi_C - \phi_B}{2}\right)\gamma_3\left(\gamma_2 - \gamma_1\right)\right]. \tag{3.21}$$

In this example the linear combination $(\gamma_1+\gamma_2)/\sqrt{2}$ is the remaining Majorana mode missing from the Hamiltonian. The linear combination $\sqrt{\gamma_1-\gamma_2}/2$ and γ_3 fuse into an electron of finite energy.

We thus see that we need to make a choice of counting order in the wires to properly define the superconducting phases in each wire segment. Moreover, when we use the T-junction construction to braid the Majorana modes around we must make certain that we do not generate unwanted "accidental" Majorana modes. Specifically, we must make certain that we do not form π-junctions while we transport the Majorana modes in the wires.

In practice, one avoids generating π-junctions by never supplying the net-energy needed to form new topological regions with Majorana pairs at the ends; the natural $\frac{\pi}{2}$ angles in the T-junction construction avoids the fine-tuned case.

3.2.2 Majorana Exchange

We will now look at the exchange of Majorana modes in the T-junction as seen in fig. 3.6. There are two similar but different exchanges described in the figure as exchange (a)-(d) where the two Majorana modes belong to the same topological region in the wire. The other exchange is seen in the figure as (e)-(h) where the Majorana modes exchanged belong to two different topological regions. We will start by looking at the (a)-(d) exchange.

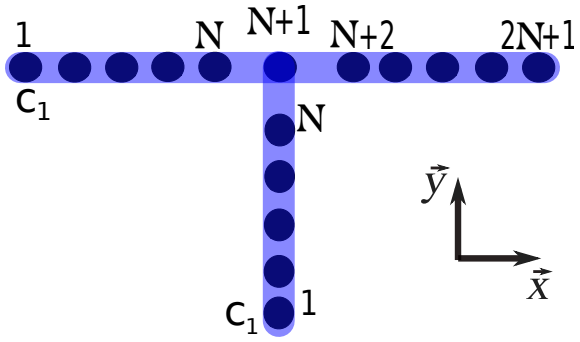

Figure 3.9: A complete T-junction, consisting of one horizontal 2N+1-site chain together with one vertical N-site chain.

To visualize the full T-junction in the language of Kitaev's chain model the T-junction must be described as consisting of **two** chains (unlike the three chains in figure 3.8). The horizontal wire consists of $2N+1$ sites and the vertical wire consists of N sites. The centre of the junction consists of a single site, with an effective site number of $N+1$ in the horizontal wire and we will identify it with the same site number $(N+1)$ for the vertical wire in the Kitaev Hamiltonian. The numbering follows the previously established convention of increasing site numbering "left to right" and "bottom to top".

We will call the spinless electron operators in the **horizontal wire** c_x and the corresponding electron operators in the **vertical wire** c_y. We can now write down the full Kitaev Hamiltonian for the T-junction:

$$\begin{aligned} H = \; & -\sum_{x=1}^{2N+1} \mu_x \, c_x^\dagger c_x - \sum_{x=1}^{2N} [t_x c_x^\dagger c_{x+1} + t_x c_{x+1}^\dagger c_x + |\Delta| \, e^{i\phi} c_x c_{x+1} + |\Delta| \, e^{-i\phi} c_{x+1}^\dagger c_x^\dagger] \\ & -\sum_{y=1}^{N} \mu_y \, c_y^\dagger c_y - \sum_{y=1}^{N} [t_y c_y^\dagger c_{y+1} + t_y c_{y+1}^\dagger c_y + \left|\hat{\Delta}\right| e^{i\hat{\phi}} c_y c_{y+1} + \left|\hat{\Delta}\right| e^{-i\hat{\phi}} c_{y+1}^\dagger c_y^\dagger], \\ & c_{x+1} \equiv c_{y+1}, \end{aligned} \tag{3.22}$$

where μ_x, Δ and ϕ ($\mu_y, \hat{\Delta}$ and $\hat{\phi}$) is the chemical potential, superconducting gap and phase, respectively, in the horizontal (vertical) chain.

This Hamiltonian describes the full T-junction system in the Kitaev chain model. Now we will make the simplification that we assume $t = |\Delta|$ as we have done before, see eq. (3.3). An additional assumption we make is that the superconducting phase ϕ in the horizontal wire and the superconducting phase $\hat{\phi}$ in the vertical wire do not differ by an integer multiple of π so as to avoid unwanted π-junctions. (In an experimental setting this would be simple to ensure since the T-junction we consider here have the two wires perpendicular and as such the relative phase difference would be $\frac{\pi}{2}$, far from the π-junction limit.)

We will also follow Alicea et al. [1] in choosing to write the pairing terms in the Kitaev chain model as $-te^{i\phi}c_x c_{x+1}$ and remembering that $t = |\Delta|$. The Hamiltonian now has the form:

$$
\begin{aligned}
H = &- \sum_{x=1}^{2N+1} \mu_x \, c_x^\dagger c_x - \sum_{y=1}^{N} \mu_y \, c_y^\dagger c_y \\
&+ \sum_{x=1}^{2N} t_x \left(e^{-i\frac{\phi}{2}} c_x^\dagger + e^{i\frac{\phi}{2}} c_x \right) \left(e^{-i\frac{\phi}{2}} c_{x+1}^\dagger - e^{i\frac{\phi}{2}} c_{x+1} \right) \\
&+ \sum_{y=1}^{N} t_y \left(e^{-i\frac{\hat{\phi}}{2}} c_y^\dagger + e^{i\frac{\hat{\phi}}{2}} c_y \right) \left(e^{-i\frac{\hat{\phi}}{2}} c_{y+1}^\dagger - e^{i\frac{\hat{\phi}}{2}} c_{y+1} \right).
\end{aligned} \tag{3.23}
$$

We do this to more directly illustrate the phase dependence governing the topological regions. As was discussed before, the superconducting phase in the pairing terms of the Kitaev chain is defined in accordance with a chosen direction ($-t_x e^{i\phi} c_x c_{x+1} \rightarrow -t_x e^{i(\phi+\pi)} c_{x+1} c_x$, and similarly for the $\hat{\phi}$ terms). This property will be used in the following exploration of the Majorana exchange properties, where for the sake of convenience, different segments of the wires will use different choices of directions (with phases defined accordingly).

Exchange of Majorana modes γ_1 and γ_2 from fig. 3.6 (a)-(d)

When the Majorana modes to be exchanged belong to the same topological region we will employ a convention that the superconducting phases are labelled as follows: $\phi + \pi$ in the left half of the horizontal wire, $\hat{\phi} + \pi$ in the vertical wire, and ϕ in the right half of the horizontal wire. When we do this we have to be careful and remember that we need to avoid creating a π-junction. We will extend the current model to include a small area close to the intersection between the three wire segments where the superconducting phases change smoothly in order to avoid this problem, in practice we avoid this by making sure that we never supply the required energy to create an unwanted Majorana pair (new topological region).

The superconducting phases will also be held fixed, however this is not a necessary requirement for the theoretical description of the system. This choice reflects what we would do in practice, holding the perpendicular magnetic field fixed. The remaining parameters that we can vary in order to move the Majorana modes around the wires are then μ_x, μ_y, t_x and t_y. In practise the transport of the Majorana modes would be done by applying local voltage gates as described in section 3.1.2. In our Hamiltonian, eq. (3.23), the equivalent action will be performed by varying the chemical potentials μ_x and μ_y together with corresponding shifts of t_x and t_y. For the sake of clarity and convenience the change of these parameters will be done by changing a single parameter at the **precise location** where we are currently transporting the topological region. We introduce this parameter λ as follows: $t_x \rightarrow t_x(\lambda)$ (or $t_y \rightarrow t_y(\lambda)$) and $\mu_x \rightarrow \mu_x(\lambda)$ (or $\mu_y \rightarrow \mu_y(\lambda)$) [1].

The topological region in the wire using the Hamiltonian of eq. (3.31) will be defined by the region fulfilling the condition

$$
\begin{aligned}
&\mu_i = 0, \\
&t_i = t > 0, \qquad i = (x,y).
\end{aligned} \tag{3.24}
$$

In contrast, the non-topological region will be defined by

$$\begin{aligned} &t_i = 0, \\ &\mu_i = \mu > 0, \qquad i = (x,y). \end{aligned} \tag{3.25}$$

To transport these regions along the wires, we need to dynamically change the μ_i and t_i by introducing a "time" parameter λ as follows:

$$\begin{aligned} &\mu_i(\lambda) \text{ and } t_i(1-\lambda), \\ &t_i(\lambda) \text{ and } \mu_i(1-\lambda), \\ &\lambda : [0 \to 1]. \end{aligned} \tag{3.26}$$

This is best understood by means of an example: We look at the starting configuration of figure 3.6, (a), and we see that the horizontal wire is in a topological state while the vertical wire is not. Using our full Kitaev chain description, remembering our choice of superconducting phases from before, the (a) configuration is then described by the Hamiltonian

$$\begin{aligned} H(\lambda_{(a)}) = -\mu_y \sum_{y=1}^{N} c_y^\dagger c_y + \sum_{x=1}^{2N} t_x \left(e^{-i\frac{\phi_x}{2}} c_x^\dagger + e^{i\frac{\phi_x}{2}} c_x \right) \left(e^{-i\frac{\phi_x}{2}} c_{x+1}^\dagger - e^{i\frac{\phi_x}{2}} c_{x+1} \right), \\ \phi_x = \phi + \pi \quad \text{for } x \leq N, \\ \phi_x = \phi \qquad \text{for } x \geq N+1. \end{aligned} \tag{3.27}$$

We here see that the μ_x and t_y terms from eq. (3.23) are zero while the μ_y and t_x terms are constants larger than zero, as described in eqs. (3.24) and (3.25). From this we find the Majorana modes as expected:

$$\begin{aligned} \gamma_1(\lambda_{(a)}) &= e^{\left(-i\frac{\phi+\pi}{2}\right)} c_1^\dagger \; + e^{\left(i\frac{\phi+\pi}{2}\right)} c_1, \\ \gamma_2(\lambda_{(a)}) &= e^{\left(-i\frac{\phi}{2}\right)} c_{(2N+1)}^\dagger \; + e^{\left(i\frac{\phi}{2}\right)} c_{(2N+1)}, \end{aligned} \tag{3.28}$$

simply by noting that the linear combinations of electron operators on the right-hand sides of eq. (3.28) are missing from the Hamiltonian (cf. eq. (A.8) in the appendix).

To transport the Majorana modes we will now use eq. (3.26). We will first look at the transport of the leftmost Majorana mode rightward to the intersection of the wires. As this transport amounts to moving the topological region step-by-step to the right, the terms we use are the following:

$$\begin{aligned} \mu_1 &= \mu(\lambda), \\ t_1 &= t(1-\lambda). \end{aligned} \tag{3.29}$$

When λ goes from 0 to 1, the Hamiltonian shifts the topological region one step to the right, and by that the left Majorana mode moves with it (the right Majorana mode is clearly unaffected).

At this point Majorana mode γ_1 is

$$\gamma_1(\lambda_2) = e^{\left(-i\frac{\phi+\pi}{2}\right)}c_2^\dagger \; + e^{\left(i\frac{\phi+\pi}{2}\right)}c_2. \tag{3.30}$$

This step-by-step process is repeated until we arrive at the configuration (b) in figure 3.6. For this configuration, the Hamiltonian is given by

$$\begin{aligned} H(\lambda_{(b)}) \; = - \sum_{x=1}^{N} \quad \mu_x \, c_x^\dagger c_x \; + \sum_{x=N+1}^{2N} t_x \left(e^{-i\frac{\phi}{2}}c_x^\dagger + e^{i\frac{\phi}{2}}c_x\right)\left(e^{-i\frac{\phi}{2}}c_{x+1}^\dagger - e^{i\frac{\phi}{2}}c_{x+1}\right) \\ + \sum_{x=1}^{N} \quad t_y \left(e^{-i\frac{\hat{\phi}+\pi}{2}}c_y^\dagger + e^{i\frac{\hat{\phi}+\pi}{2}}c_y\right)\left(e^{-i\frac{\hat{\phi}+\pi}{2}}c_{y+1}^\dagger - e^{i\frac{\hat{\phi}+\pi}{2}}c_{y+1}\right), \end{aligned} \tag{3.31}$$

with corresponding Majorana modes

$$\begin{aligned} \gamma_1(\lambda_{(b)}) = \; s_1 \left[e^{\left(-i\frac{\hat{\phi}+\pi}{2}\right)}\hat{c}_1^\dagger \; + e^{\left(i\frac{\hat{\phi}+\pi}{2}\right)}\hat{c}_1\right], \\ \gamma_2(\lambda_{(b)}) = \; \gamma_2(\lambda_{(a)}), \end{aligned} \tag{3.32}$$

where s_1 denotes a multiplicative sign factor. This sign factor reflects the uncertainty of whether or not the Majorana mode picks up a minus sign during the transport from (a) to (b). The origin of this possible sign difference lies in the spinor nature of the Majorana mode: any 2π rotation of the Majorana mode will result in a sign flip. As the Majorana mode moves from the left part of the horizontal wire down into the vertical wire, the superconducting phase shifts from $(\phi+\pi)$ to $\hat{\phi}+\pi$. This shift in superconducting phase would be the source of the sign change, as it would be the only thing changing for the Majorana mode as it travels in the real experimental system.

This type of potential sign change is an unavoidable aspect of the Majorana properties. As such, we will need to address a potential sign change in every step of the Majorana exchange, (a) to (d). These sign changes depend on the specifics of the exchange system (which could in principle be derived for each potential case), unless we can find some general rule using only the basic information we have about the Kitaev system and the Majorana properties. We wish to find a general rule for the Majorana exchange and to that end we will make use of a trick: We will deform the system and look closely at the intersection of the two wires (close to the $(N+1)$:st site). Specifically, we will look at what happens when we go from (a) to (b) in a slightly deformed Hamiltonian which smoothly connects to eq. (3.22). Suppose that instead of the superconducting phases jumping discontinuously between the horizontal and vertical wires, the phase in the vertical wire is varied spatially from $\hat{\phi}+\pi$ at the bottom to $\phi+\pi$ at the top[1]. The phase shift is assumed to occur very close to the intersection. This deformation is illustrated below in figure 3.10.

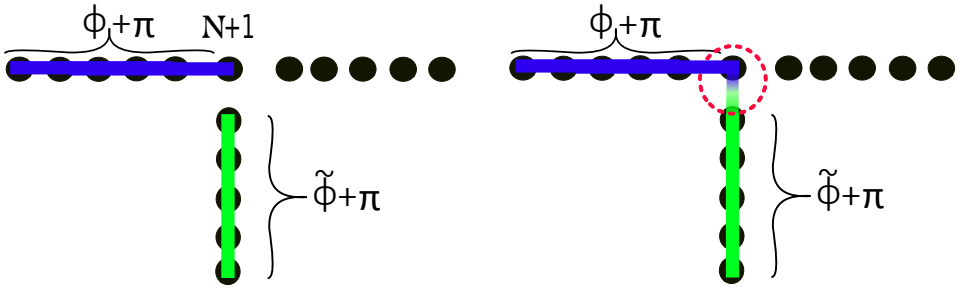

(a) The original T-junction.

(b) The slightly deformed T-junction with the smooth transition of the superconducting phase circled in red.

Figure 3.10: Deformation of the T-junction with the relevant superconducting phases illustrated as blue and green.

To distinguish this slightly modified system from the original Kitaev chain system, we now rename the Majorana modes as

$$\begin{aligned}\gamma_1'(\lambda) &= e^{\left(-i\frac{\phi(\lambda)}{2}\right)}c_1(\lambda)^\dagger + e^{\left(i\frac{\phi(\lambda)}{2}\right)}c_1(\lambda),\\ \gamma_2'(\lambda) &= e^{\left(-i\frac{\phi(\lambda)}{2}\right)}c_2^\dagger(\lambda) + e^{\left(i\frac{\phi(\lambda)}{2}\right)}c_2(\lambda).\end{aligned} \tag{3.33}$$

In this modified system the superconducting phase for $\gamma_1'(\lambda)$ changes from $\phi+\pi$ to $\hat{\phi}+\pi$ as well. This change of phase can occur in two ways, clockwise or counter-clockwise. In fig. (3.11) we visualise the range of superconducting phases available to the Majorana mode and the two ways of shifting from one phase to the other.

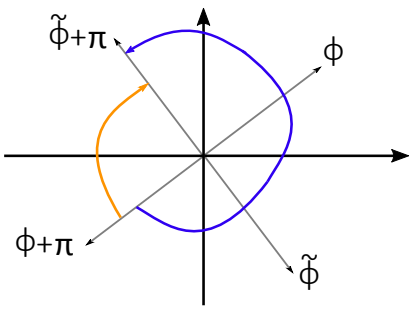

Figure 3.11: Two ways the superconducting phase can shift during transport.

The difference between the two ways of shifting the phase is in total a 2π difference. This unavoidably results in a net shift of the sign for the Majorana mode due to its spinor nature. So we can now say, completely generally, that over the range of available phases, the two ways that the phase can change, the net difference is always a change of sign for the Majorana mode.

Based on this observation we can ignore the specifics of the underlying system (we only use the basic spinor nature of the Majorana mode), and summarise the 2π difference in travel path by introducing a branch cut in the phase space of figure 3.11.

We are free to choose where we place this branch cut, and here we chose to place it along the positive "x" axis for the sake of convenience. With this choice of branch cut, we can now trace the history of the superconducting phase for the Majorana mode in the (a)-(b) system. We illustrate this in fig. (3.12). By the given choice of branch cut, the path

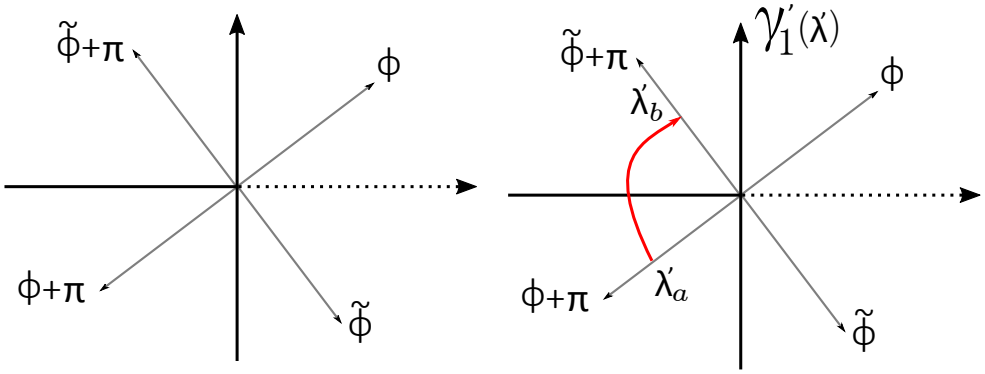

(a) Phase space with branch cut along the positive x-axis.

(b) Phase for Majorana mode $\gamma_1'(\lambda)$ as the system moves from (a)-(b) in fig. 3.6.

Figure 3.12

of the phase is forced to run clockwise (red curve in fig. 3.11 (b)). In this way we avoid generating a π-junction in the system, as would have been the case if we had chosen a path going counterclockwise from $\phi + \pi$ to ϕ.

Experimental note: an unwanted π-junction will generate a new non-topological region with two Majorana modes at its ends. Since in practice it requires energy to form this region, [cf. eq. (3.17)], we require that in our idealized model the phase *must not* pass through ϕ and as a result the phase changes as shown i figure 3.12.

The step-by-step process introduced above is now to be repeated when we move γ_2 in the (b) to (c) configurations. In this way we end up with a transformed γ_2 with a possible sign change, just like the one seen in eq. (3.32). The underlying superconducting phase change is investigated by using the same trick as before. Then we monitor the change of the phase for $\gamma_2'(\lambda)$ as we did just above, and make sure to add a phase 2π if we cross the branch cut (see fig. 2.2). The same sequence is then carried out for γ_1 in the last transport, from the (c) configuration to the (d) configuration.

To reduce clutter, we will only show the phase diagrams for these steps as it is the final result we are interested in.

We have now completed the Majorana exchange when the Majorana modes are in the same topological region ((a)-(d) in fig. 3.6). The step-by-step treatment results in the final Majorana modes

$$\begin{aligned}\gamma_1(\lambda_{(a)}) &= s_1\, s_3 \left[e^{\left(-i\frac{\phi}{2}\right)} c^\dagger_{(2N+1)} \; + e^{\left(i\frac{\phi}{2}\right)} c_{(2N+1)} \right], \\ \gamma_2(\lambda_{(a)}) &= \quad s_2 \left[e^{\left(-i\frac{\phi+\pi}{2}\right)} c_1^\dagger \; + e^{\left(i\frac{\phi+\pi}{2}\right)} c_1 \right],\end{aligned} \tag{3.34}$$

where s_1, s_2 and s_3 are multiplicative sign factors. By identifying the phases and locations of the Majorana modes we see that the interchange of the Majorana modes γ_1 and γ_2 results in:

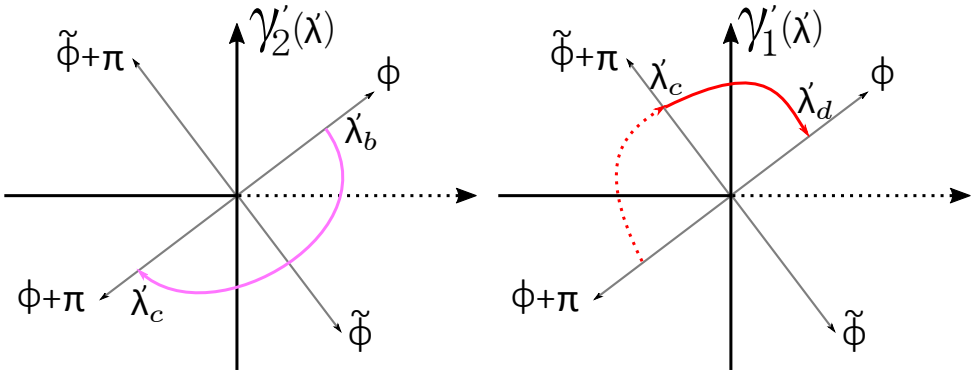

(a) Phase for Majorana mode $\gamma_2'(\lambda)$ as the system changes from (b) to (c) in fig. 3.6.

(b) Phase for Majorana mode $\gamma_1'(\lambda)$ as the system changes from (c) to (d) in fig. 3.6.

Figure 3.13

$$\begin{aligned} \gamma_1 &\to (s_1 s_3)\, \gamma_2, \\ \gamma_2 &\to (s_2)\, \gamma_1. \end{aligned} \tag{3.35}$$

Looking back at figures 3.12 and 3.13 we see that the phases for γ_1' and γ_2' both rotate the same way (clockwise in this case), and the combined rotation amounts to a full 2π rotation. This means that either the $s_1\, s_3$ combination changes the sign of the Majorana mode, or the s_2 changes the sign of that Majorana mode. This is an inescapable conclusion based solely on the fundamental spinor properties of the Majorana mode and the experimentally necessary requirement of having no π-junctions. We thus conclude that

$$\begin{aligned} \gamma_1 &\to \quad s\gamma_2, \\ \gamma_2 &\to -s\gamma_1, \end{aligned} \tag{3.36}$$

for some sign s that depends on the specific choice of the branch cut and the convention one uses for the increasing site numbering in the chains as explained after eq. (3.23). For the sake of clarity we set s to unity,

$$\begin{aligned} \gamma_1 &\to \quad \gamma_2, \\ \gamma_2 &\to -\gamma_1. \end{aligned} \tag{3.37}$$

This demonstrates that the interchange of two Majorana modes in our T-junction produces the same exchange statistics as the Majorana modes trapped in vortices [cf. section 2.1.5].

We have only one glaring question to answer before we follow the same step-by-step treatment of the (e)-(h) system: Is the result obtained for the modified system actually usable for our original discontinuous one. The motivation for why we can use the $\gamma_i'(\lambda)$ for the phase investigation and claim that the result for our original system (with Majorana modes γ_i) boils down to the fact that the exchange statistics, eq. (3.36), is a universal property of this class of systems. This is so since no band gap is closed by our slight modification. Importantly, the modification itself lies closer to the experimental reality since the shift in phase close to the intersection is not a discrete jump but a (small) continuous transition.

Exchange of Majorana modes γ_1 and γ_2 from fig. 3.6 (e)-(h)

This section will be short due to the fact that the necessary step-by-step process is similar to that described in the previous section. As in the previous section the (e) to (h) exchange will be described by using the initial Majorana modes for reference and then followed by a phase-shift analysis. A note will be made about the special situation arising at the intersection when all three wire segments are topological. (This happens halfway through the (f)-(g) transport).

The choices made concerning the topological phases are as follows: The phase in the left half of the horizontal wire will be called ϕ, the phase in the vertical wire will be called $\hat{\phi}+\pi$, and finally the phase in the right section of the horizontal wire will be called $\phi+\pi$. Apart from this, the Kitaev chain Hamiltonian is the same as in eq. (3.27).

The initial Majorana modes seen in fig. 3.6(e) reside in two separate topological regions and are described by the following:

$$\begin{aligned}\gamma_1(\lambda_{(e)}) &= e^{\left(-i\frac{\phi}{2}\right)}c_A^\dagger + e^{\left(i\frac{\phi}{2}\right)}c_A,\\ \gamma_2(\lambda_{(e)}) &= e^{\left(-i\frac{\phi+\pi}{2}\right)}c_B^\dagger + e^{\left(i\frac{\phi+\pi}{2}\right)}c_B.\end{aligned} \tag{3.38}$$

The sites A and B are shown below in fig. 3.14.

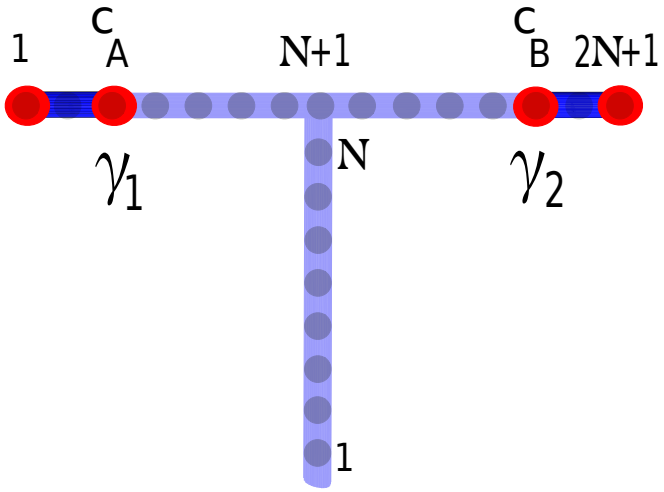

Figure 3.14

Referring to fig. 3.6(e), after the first transport is completed, we arrive at the configuration (f) and in this case the Majorana modes are given by

$$\begin{aligned}\gamma_1(\lambda_{(f)}) &= s_1 \left[e^{\left(-i\frac{\hat{\phi}+\pi}{2}\right)} \hat{c}_1^\dagger \; + e^{\left(i\frac{\hat{\phi}+\pi}{2}\right)} \hat{c}_1 \right], \\ \gamma_2(\lambda_{(f)}) &= \gamma_2(\lambda_{(e)}),\end{aligned} \tag{3.39}$$

where s_1 denotes a multiplicative sign factor. While the Majorana modes are transported along the wires by the same kind of step-by-step process as described in the (a)-(d) example, there is one specific move that is different. In the (f)-(g) transport, moving γ_2 to the left, the phase changes from $\phi + \pi$ on the right side to ϕ on the left side while passing $\hat{\phi} + \pi$ in between. In the intermediate state of the (f)-(g) transport, all wire segments are in a topological state. This leads to the formation of a π-junction at the centre of the T-junction. To understand what happens we recall the example given after eq. (3.20). In that case, with all three wire segments being in the topological phase we can allow for a π-junction between two wire segments since the third segment can hold the Majorana mode. No new Majorana modes are forced to be created. (Experimentally we just avoid supplying the energy required to generate a new topological region). The π-junction separates the γ_2 in the horizontal wire from any possible interactions in the vertical wire.

The Majorana mode at the centre of the T-junction (the one missing from the Hamiltonian as usual) is then expressed as

$$\gamma_2'(\lambda_{centre}) = \frac{1}{\sqrt{2}} \left[e^{-i(\frac{\hat{\phi}+\pi}{2})} \left(-c_N^\dagger + c_{N+2}^\dagger \right) + e^{i(\frac{\hat{\phi}+\pi}{2})} \left(-c_N + c_{N+2} \right) \right]. \tag{3.40}$$

As seen from this formula, we now have a negative sign on the electron operator belonging to the right part of the horizontal chain, $-c_N$. This extra minus sign which the Majorana mode picks up when passing the centre of the T-junction has the effect of ensuring that the exchange properties are the ones we expect. As we see in figure 3.15, the phases acquired for $\gamma_1'(\lambda)$ and $\gamma_2'(\lambda)$ when taking this path results in a vanishing total phase shift. Either both Majorana modes change sign, or neither one does. It is the change in sign resulting from the crossing of the centre of the T-junction that ends up making all the difference. The final exchanged Majorana modes are then given by

$$\begin{aligned}\gamma_1(\lambda_{(h)}) &= s_1 s_3 \left[e^{\left(-i\frac{\phi+\pi}{2}\right)} c_B^\dagger \; + e^{\left(i\frac{\phi+\pi}{2}\right)} c_B \right], \\ \gamma_2(\lambda_{(h)}) &= -s_2 \left[e^{\left(-i\frac{\phi}{2}\right)} c_A^\dagger \; + e^{\left(i\frac{\phi}{2}\right)} c_A \right], \\ (s_1 s_3) &= s_2,\end{aligned} \tag{3.41}$$

where s_1, s_2 and s_3 are multiplicative sign factors. So finally we arrive at the expected exchange property:

$$\begin{aligned}\gamma_1 &\rightarrow \quad s\gamma_2, \\ \gamma_2 &\rightarrow -s\gamma_1,\end{aligned} \tag{3.42}$$

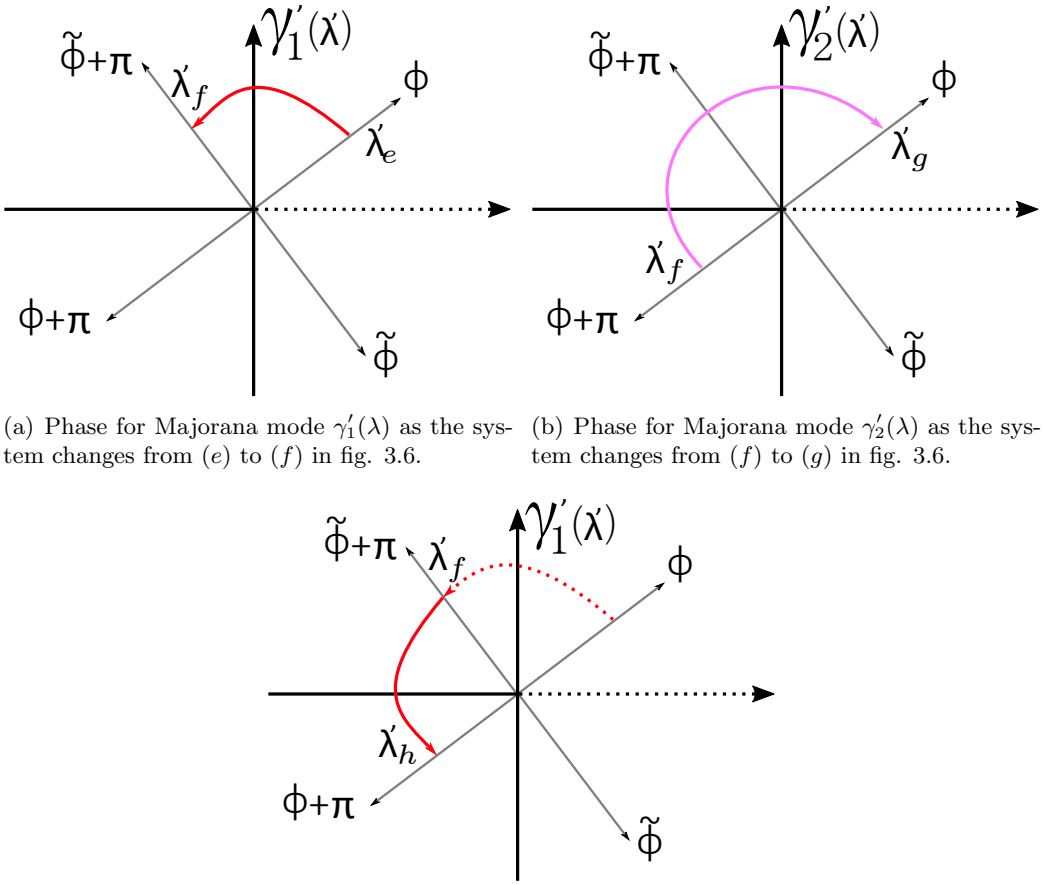

(a) Phase for Majorana mode $\gamma'_1(\lambda)$ as the system changes from (e) to (f) in fig. 3.6.

(b) Phase for Majorana mode $\gamma'_2(\lambda)$ as the system changes from (f) to (g) in fig. 3.6.

(c) Phase for Majorana mode $\gamma'_1(\lambda)$ as the system changes from (g) to (h) in fig. 3.6.

Figure 3.15

where the sign s depends on the choice of branch cut and the convention one uses for the increasing site numbering in the chains as explained after eq. (3.23). For the sake of clarity we set s to unity, resulting in

$$\begin{aligned} \gamma_1 &\rightarrow \quad \gamma_2, \\ \gamma_2 &\rightarrow -\gamma_1. \end{aligned} \tag{3.43}$$

This is exactly the same conclusion we arrived at in the (a)-(d) case.

3.2.3 Non-Abelian Statistics

Summarising the results from the previous sections we have identified Majorana modes located at the edges of wire segments in a topological state. By exchanging the Majorana modes through the application of gate voltages they are found to exhibit the expected exchange statistics. This statistics can be expressed as

$$\begin{aligned} \gamma_i &\rightarrow s_{ij}\gamma_j, \\ \gamma_j &\rightarrow -s_{ij}\gamma_i, \end{aligned} \tag{3.44}$$

where the sign s_{ij} depends on the specifics of our chosen system. We can introduce an operator U_{ij} that generates the exchanges in eq. (3.44):

$$U_{ij} = \frac{1 + s_{ij}\gamma_j\gamma_i}{\sqrt{2}}. \tag{3.45}$$

We now use U_{ij} to generate the exchanges in eq. (3.44):

$$\begin{aligned} \gamma_i \rightarrow U_{ij}\,\gamma_i\,U_{ij}^\dagger &= \frac{1}{2}(1 + s_{ij}\gamma_j\gamma_i)\,\gamma_i\,(1 - s_{ij}\gamma_j\gamma_i) \quad = \frac{1}{2}(\gamma_i + s_{ij}\gamma_j)(1 - s_{ij}\gamma_j\gamma_i) \\ &= \frac{1}{2}(\gamma_i - s_{ij}\gamma_i\gamma_j\gamma_i + s_{ij}\gamma_j - s_{ij}^2\gamma_i) = \frac{1}{2}(\gamma_i + s_{ij}\gamma_j + s_{ij}\gamma_j - \gamma_i) \\ &= s_{ij}\gamma_j, \\ \gamma_j \rightarrow U_{ij}\,\gamma_j\,U_{ij}^\dagger &= \frac{1}{2}(1 + s_{ij}\gamma_j\gamma_i)\,\gamma_j\,(1 - s_{ij}\gamma_j\gamma_i) = \frac{1}{2}(\gamma_j - s_{ij}\gamma_i)(1 - s_{ij}\gamma_j\gamma_i) \\ &= \frac{1}{2}(\gamma_j - s_{ij}\gamma_i - s_{ij}\gamma_i - s_{ij}^2\gamma_j) = \frac{1}{2}(\gamma_j - s_{ij}\gamma_j - s_{ij}\gamma_j - \gamma_j) \\ &= -s_{ij}\gamma_i. \end{aligned} \tag{3.46}$$

The non-abelian nature of the Majorana modes are expressed by the following operator commutator:

$$\left[U_{ij},\, U_{jk}\right] = s_{ij}s_{jk}\gamma_i\gamma_k. \tag{3.47}$$

If we now make the choice $s_{ij} = -1$, the exchange operator becomes $U_{ij} = (1 - \gamma_i\gamma_j)\sqrt{2}$ (this choice will be made for the *counterclockwise rotation* in chapter 4). The effect on the vacuum state in eq. (2.31) and the ground state in eq. (2.34) when exchanging γ_1 and γ_2 is then

$$\begin{aligned} U_{12}\,|0_1 0_2\rangle &= \frac{1}{\sqrt{2}}(1 - i)\,|0_1 0_2\rangle\,, \\ U_{12}\,|1_1 1_2\rangle &= \frac{1}{\sqrt{2}}(1 + i)\,|1_1 1_2\rangle\,. \end{aligned} \tag{3.48}$$

This is shown in appendix eq. (A.14).

To illustrate what happens when we interchange two Majorana modes originating from *different* electron operators we will now investigate a two-particle state with electron operators

c_1 and c_2 using eq. (2.42):

$$\begin{aligned} c_1 &= \frac{1}{\sqrt{2}}(\gamma_1 + i\gamma_2), \\ c_1^\dagger &= \frac{1}{\sqrt{2}}(\gamma_1 - i\gamma_2), \\ c_2 &= \frac{1}{\sqrt{2}}(\gamma_3 + i\gamma_4), \\ c_2^\dagger &= \frac{1}{\sqrt{2}}(\gamma_3 - i\gamma_4). \end{aligned} \tag{3.49}$$

Using these operators we now look at the exchange operator U_{23} (exchanging Majorana mode γ_2 and γ_3) acting on the number states $|0_1 0_2\rangle$ and $|1_1 1_2\rangle$:

$$\begin{aligned} U_{23}\,|0_1 0_2\rangle &= \frac{1}{\sqrt{2}}\,(1 - \gamma_2\gamma_3)\,|0_1 0_2\rangle = \frac{1}{\sqrt{2}}\left(|0_1 0_2\rangle - i\,|1_1 1_2\rangle\right), \\ U_{23}\,|1_1 1_2\rangle &= \frac{1}{\sqrt{2}}\,(1 - \gamma_2\gamma_3)\,|1_1 1_2\rangle = \frac{1}{\sqrt{2}}\left(-i\,|0_1 0_2\rangle + |1_1 1_2\rangle\right). \end{aligned} \tag{3.50}$$

The full derivation is found in the appendix [cf. eqs. (A.4), (A.5), (A.15) and (A.16)]. Here we see that the filled and empty states mix. This will be important for the the quantum gates, investigated in chapter 4.

Using eq. (3.47) the commutator for these two exchange operators is then

$$[U_{12},\, U_{23}] = \gamma_1\gamma_3. \tag{3.51}$$

3.3 The Wire Network

From the analysis of the T-junction in the previous sections it is suggestive that it should in principle be straightforward to scale up the design to any desired size so as to obtain the required number of Majorana modes to be used for quantum computations: The basic ingredients are an ordinary s-wave superconductor, nanowires [33] and and a magnetic field. The process of scaling up the T-junction construct is displayed in fig. (3.16).

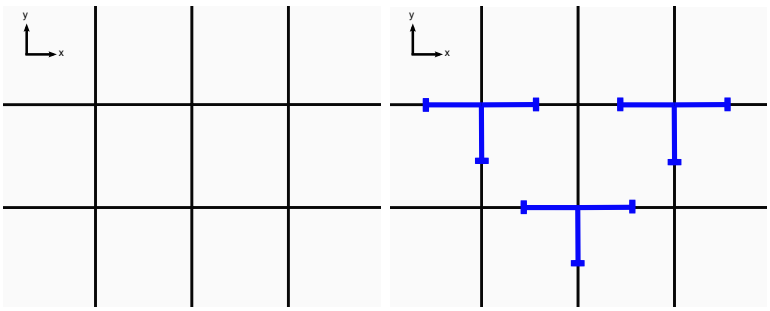

(a) Snapshot of a nanowire network.

(b) Arbitrarily chosen T-junctions usable for braiding.

Figure 3.16: A network of nanowires.

4

Quantum Gates

In chapter 3 we saw that by making use of the T-junction construction one is able to interchange Majorana modes. Now we ask the question how we can exploit this property to perform quantum operations. The answer is to use the exchange operation to braid the Majorana modes which comprise a qubit state in the wire network. Correctly braiding the Majorana modes applies a quantum gate to the state.

4.1 Network to Diagram

We begin by looking at the operations we can perform by using the basic exchange operation that we studied in chapter 3.2. The exchange operation seen in fig. (3.6) changed the positions of the two Majorana modes while at the same time changing the sign of one of the modes:

$$\begin{aligned} \gamma_1 &\rightarrow \quad \gamma_2, \\ \gamma_2 &\rightarrow -\gamma_1. \end{aligned} \tag{4.1}$$

This result was derived in section 3.2.2 [cf. eqs. (3.37) and (3.43)] and corresponds to a **counterclockwise** exchange in our chosen basis [cf. eq. (2.54)]. This exchange can be described in two ways, as a result of applying an exchange operator or performing a braid operation.

4.1.1 Exchange Operator

The operator generating the exchange was introduced in chapter 3.2.3 as eq. (3.45):

$$U_{ij} = \frac{1}{\sqrt{2}}(s_{ij}\gamma_j\gamma_i). \tag{4.2}$$

In the general case seen in eq. (3.45), the sign operator s_{ij} depends on the specifics of the underlying system. Now we specify this to the counterclockwise exchange in eq. (4.1):

$$U_{12} = \frac{1}{\sqrt{2}}(1 - \gamma_1\gamma_2). \tag{4.3}$$

Using eq. (2.60) we see that the **braid operator** U_{12} generates a counterclockwise exchange through

$$\begin{aligned} U_{12}\ \gamma_1\ U_{12}^\dagger &= \ \ \gamma_2, \\ U_{12}\ \gamma_2\ U_{12}^\dagger &= -\gamma_1. \end{aligned} \tag{4.4}$$

4.1.2 Braid Diagram

The other description of the exchange in eq. (4.1) uses a braid diagram. A braid diagram for this system is constructed by strings connected to points, with the points corresponding to Majorana modes. In the braid diagrams used in this thesis, time progresses in the downward direction and the two types of braids, clockwise and counterclockwise, are distinguished by which string is braided over the other.

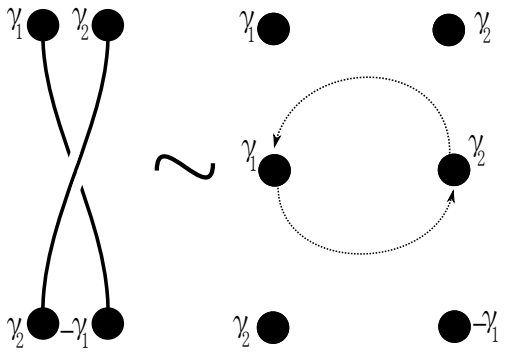

Figure 4.1: Braid diagram showing the **counterclockwise** exchange of γ_1 and γ_2.

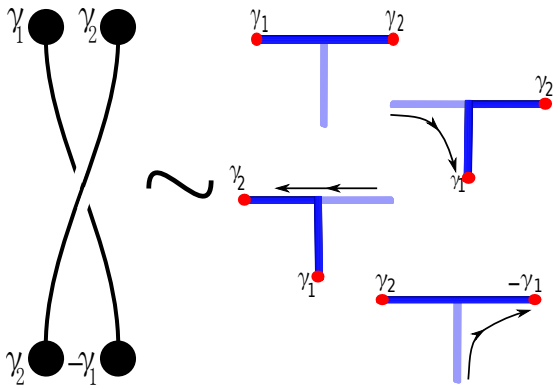

Figure 4.2: Braid diagram showing the counterclockwise exchange of γ_1 and γ_2, compared with the equivalent T-junction exchange.

4.1.3 Clockwise Exchange

We now illustrate the corresponding **clockwise** exchange. The clockwise exchange of Majorana modes γ_1 and γ_2 reads:

$$\begin{aligned} \gamma_1 &\rightarrow -\gamma_2, \\ \gamma_2 &\rightarrow \ \ \gamma_1. \end{aligned} \tag{4.5}$$

The corresponding braid operator is given by

$$\hat{U}_{12} = \frac{1}{\sqrt{2}}(1 + \gamma_1\gamma_2), \tag{4.6}$$

with the braid diagram in fig. (4.3).

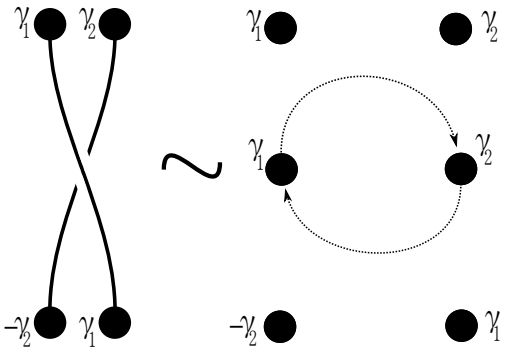

Figure 4.3: Braid diagram showing the clockwise exchange of γ_1 and γ_2.

4.1.4 Composite Operations

The elementary exchange allows us to perform more complex operations. For example, we can perform a full rotation of a state by two successive applications of the same exchange.

In operator notation:

$$\begin{aligned} U_{12}^2\ \gamma_1\ (U_{12}^2)^\dagger &= (-\gamma_1\gamma_2)\,\gamma_1\,(-\gamma_1\gamma_2)^\dagger = -\gamma_1, \\ U_{12}^2\ \gamma_2\ (U_{12}^2)^\dagger &= (-\gamma_1\gamma_2)\,\gamma_2\,(-\gamma_1\gamma_2)^\dagger = -\gamma_2. \end{aligned} \tag{4.7}$$

Note that

$$\begin{aligned} U_{12}^2\,|0_1\rangle &= (-\gamma_1\gamma_2)\,|0_1\rangle = -i\,|0_1\rangle\,, \\ U_{12}^2\,|1_1\rangle &= (-\gamma_1\gamma_2)\,|1_1\rangle = \ i\,|1_1\rangle\,, \end{aligned} \tag{4.8}$$

where the eigenvalues $\pm i$ of U_{12}^2 are derived in the appendix as eqs. (A.2, A.3)

The rotations in eq. (4.7) can be illustrated in the braid diagram in fig. (4.4).

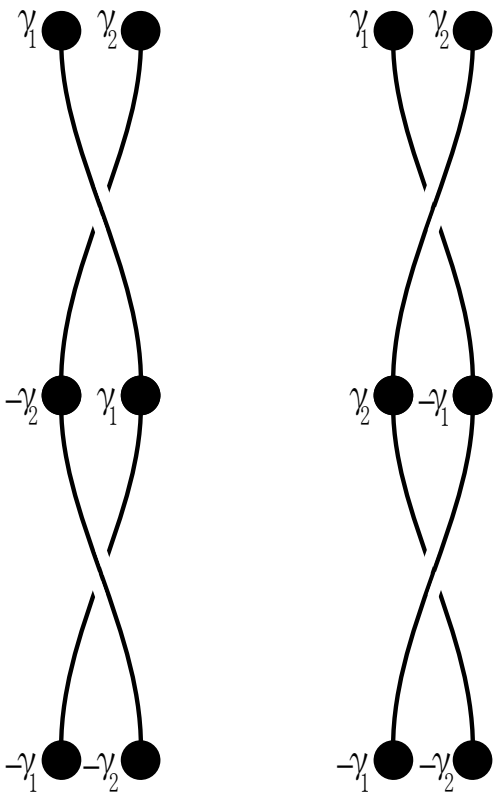

Figure 4.4: Braid diagram showing the total rotation of γ_1 and γ_2 after braiding twice.

4.1.5 Topological Qubit

To be able to use the Majorana modes for quantum computation we need to create a qubit. To generate the $|1\rangle$ state of the qubit we will use the presence of the zero-energy state introduced in the Kitaev chain when we generated a topological region [cf. eqs. (2.81) and (3.8)]:

$$\begin{aligned} \text{Majorana qubit: } & c_1 |0\rangle + c_2 |1\rangle , \\ & d_{end}^\dagger |0\rangle = |1\rangle , \\ & d_{end} |0\rangle = 0, \\ & d_{end} = \frac{1}{2} (\gamma_1 + i\gamma_2) . \end{aligned} \tag{4.9}$$

This qubit is a (topological) **physical qubit**, an effective two-level quantum system that can store quantum information where the quantum state is a superposition of two basis states $|0\rangle$ and $|1\rangle$. However, to be able to use qubits in quantum computations we must create a so-called **logical qubit**. To show that the Majorana qubit as defined above is not enough we will look at the effect of applying the braid operator to a single Majorana number state:

$$\begin{aligned} U_{12} |0\rangle &= \frac{1}{\sqrt{2}} (1 - \gamma_1\gamma_2) |0\rangle = \frac{1}{\sqrt{2}} (1 - i) |0\rangle , \\ U_{12} |1\rangle &= \frac{1}{\sqrt{2}} (1 - \gamma_1\gamma_2) |1\rangle = \frac{1}{\sqrt{2}} (1 + i) |1\rangle . \end{aligned} \tag{4.10}$$

Here we see (again) that the exchange of the two Majorana modes only results in a phase shift of the number states $|0\rangle$ and $|1\rangle$. A single Majorana qubit state is **not** enough to perform the quantum computations discussed in chapter 2.4 since the two possible braiding operations U_{12} and $U_{12}^\dagger$ do not allow us to change the qubit state itself.

4.1.6 Logical Qubit

To be able to use the topological states for quantum computation we need at least two topological qubits, involving four Majorana modes capable of forming two zero-energy fermionic occupation states $|n_1 n_2\rangle$:

$$\begin{aligned}
&\text{Logical qubit: } c_1 |\hat{0}\rangle + c_2 |\hat{1}\rangle ,\\
&\text{Logical qubit, even parity: } |\hat{0}\rangle = |0_1 0_2\rangle \text{ and } |\hat{1}\rangle = |1_1 1_2\rangle ,\\
&\text{Logical qubit, odd parity : } |\hat{0}\rangle = |0_1 1_2\rangle \text{ and } |\hat{1}\rangle = |1_1 0_2\rangle ,\\
&\qquad\qquad d_1^\dagger d_2^\dagger |\hat{0}\rangle = |\hat{1}\rangle ,\\
&\qquad\qquad d_1 d_2 |\hat{0}\rangle = 0,\\
&\qquad\qquad d_n = \frac{1}{2}\left(\gamma_{(2n-1)} + i\gamma_{(2n)}\right).
\end{aligned} \tag{4.11}$$

Here we see that we need at least two physical Majorana qubits to construct one logical qubit. In principle 2^N Majorana modes (N physical Majorana qubits) can support $N-1$ logical qubits [23]. The logical qubits are the ones we can apply gates to in order to do quantum computations.

To create a superposition of different number states we must mix Majorana modes originating from different electron states [23]. We will now consider the even-parity basis for the logical qubit and use the braid operators described in chapter 3.2.3, eq. (3.50), on the number state:

$$\begin{aligned}
U_{23} |\hat{0}\rangle &= \frac{1}{\sqrt{2}} (1 - \gamma_2\gamma_3) |00\rangle = \frac{1}{\sqrt{2}} \left(|00\rangle - i |11\rangle\right) = \frac{1}{\sqrt{2}} \left(|\hat{0}\rangle - i |\hat{1}\rangle\right),\\
U_{23} |\hat{1}\rangle &= \frac{1}{\sqrt{2}} (1 - \gamma_2\gamma_3) |11\rangle = \frac{1}{\sqrt{2}} \left(-i |00\rangle + |11\rangle\right) = \frac{1}{\sqrt{2}} \left(-i |\hat{0}\rangle + |\hat{1}\rangle\right).
\end{aligned} \tag{4.12}$$

We see that the total parity $(n_1 + n_2)$ of each state remains the same after braiding. The full calculations can be found in the appendix [cf. eqs. (A.4), (A.15) and (A.16)].

4.1.7 Matrix Notation

A useful formalism when studying quantum operations is to use **matrix notation** in the computational basis, briefly introduced in chapter 2.4 as the computational basis, where states are represented by vectors and operators by matrices

$$\begin{aligned}
&\text{Qubit state: } |\hat{0}\rangle \rightarrow \text{ Vector: } \begin{bmatrix} 1 \\ 0 \end{bmatrix}, \quad \text{Qubit state: } |\hat{1}\rangle \rightarrow \text{ Vector: } \begin{bmatrix} 0 \\ 1 \end{bmatrix},\\
&\text{Operator: } U_{12} = \frac{1}{\sqrt{2}}(1 - \gamma_1\gamma_2) \rightarrow \text{ Matrix: } \frac{1}{\sqrt{2}} \begin{bmatrix} 1-i & 0 \\ 0 & 1+i \end{bmatrix}.
\end{aligned} \tag{4.13}$$

Rewriting eq. (4.12) in matrix representation, one obtains::

$$
\begin{aligned}
U_{23}\,|\hat{0}\rangle &= \frac{1}{\sqrt{2}}\begin{bmatrix} 1 & -i \\ -i & 1 \end{bmatrix}\begin{bmatrix} 1 \\ 0 \end{bmatrix} = \begin{bmatrix} 1 \\ -i \end{bmatrix} = \frac{1}{\sqrt{2}}\Big(\ |\hat{0}\rangle - i\,|\hat{1}\rangle\Big)\,, \\
U_{23}\,|\hat{1}\rangle &= \frac{1}{\sqrt{2}}\begin{bmatrix} 1 & -i \\ -i & 1 \end{bmatrix}\begin{bmatrix} 0 \\ 1 \end{bmatrix} = \begin{bmatrix} -i \\ 1 \end{bmatrix} = \frac{1}{\sqrt{2}}\Big(-i\,|\hat{0}\rangle + |\hat{1}\rangle\Big)\,.
\end{aligned}
\tag{4.14}
$$

4.2 Quantum Gates

We will now look at how we can braid Majorana modes in the nanowire network to create quantum gates. Two quantum gates will be constructed using the braiding in the T-junction, the Pauli X-gate (or NOT gate) and the Hadamard gate. The Hadamard gate is one of three gates needed for universal quantum computations cf. chapter 2.4.1. The other two gates lies beyond the scope of this thesis as the CNOT gate is a two-qubit gate and the $\pi/8$ phase gate can not be realised by braiding alone [31].

4.2.1 Pauli X-Gate

The first quantum gate we will look at is the Pauli X-gate, a single qubit gate that was introduced in chapter 2.4 as eq. (2.79) mapping $|\hat{0}\rangle$ to $|\hat{1}\rangle$ and vice versa. We will use this gate to illustrate the utility of the braid diagram formalism compared to the T-junction description.

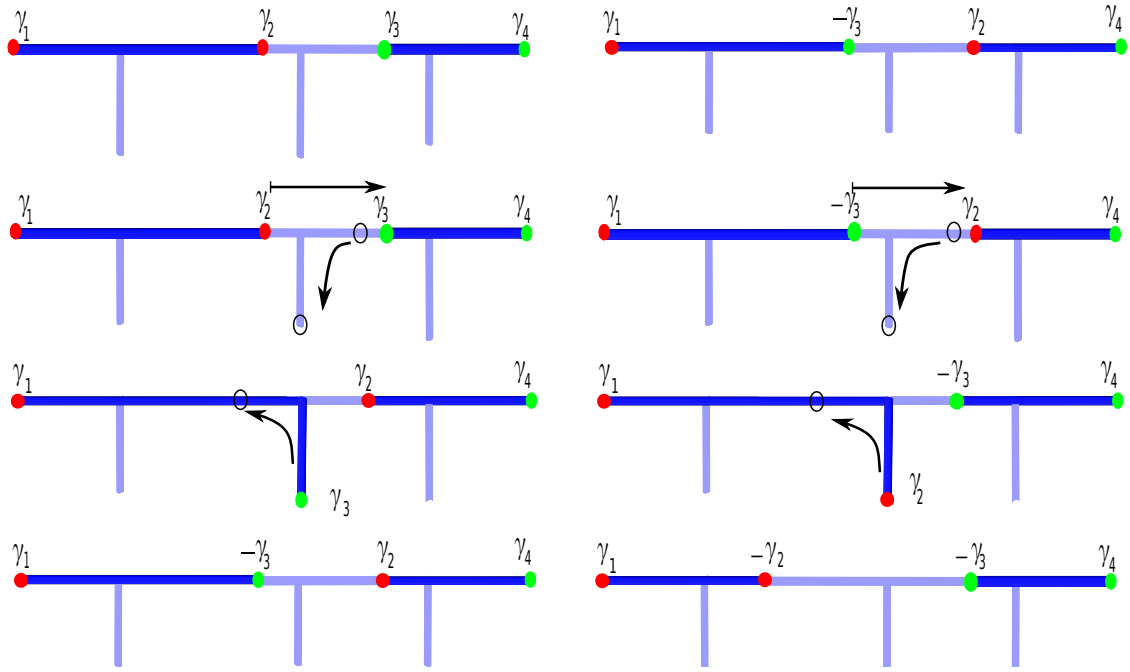

(a) Initial clockwise braid of Majorana mode γ_3 and γ_2.

(b) γ_2 and γ_3 clockwise braid.

Figure 4.5: A Pauli X-gate braid in the T-junction formalism.

Next we look at the same braiding in a braid diagram:

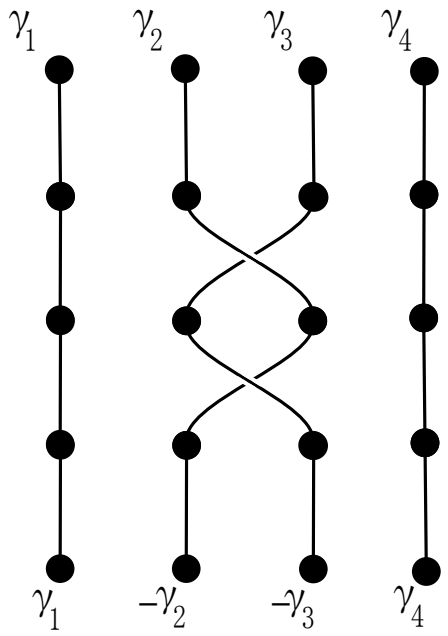

Figure 4.6: Pauli X-gate braid in the braiding diagram formalism.

Here we see that the braid diagram provides a much clearer description of the Majorana braiding process compared to the T-junction formalism.

The effect of applying the two braids in Fig. 4.6 is seen on the states in the logical qubit basis:

$$\begin{aligned} \hat{U}_{23}\hat{U}_{23}\,|\hat{0}\rangle \; &= ... = \gamma_2\gamma_3\,|\hat{0}\rangle = ... = i\,|\hat{1}\rangle\,, \\ \hat{U}_{23}\hat{U}_{23}\,|\hat{1}\rangle \; &= ... = \gamma_2\gamma_3\,|\hat{1}\rangle = ... = i\,|\hat{0}\rangle\,. \end{aligned} \tag{4.15}$$

Up to a phase, the qubit state $|\hat{0}\rangle$ becomes $|\hat{1}\rangle$ and vice versa , see appendix eqs. (A.4, A.5 and A.17) for detailed calculations.

This example shows how we can translate to a braid diagram from a T-junction braid. As this simple network can be expanded to include an arbitrary number of Majorana modes the space required to illustrate the network makes the T-junction formalism rather cumbersome. Thus when discussing more complex quantum gates, one sticks with the braiding formalism only.

4.2.2 Hadamard Gate

The Hadamard gate transforms a single qubit basis state into an equal superposition state and therefore is is often used as an initial step in quantum computations. It was introduced in chapter 2.4 as eq. (2.82).

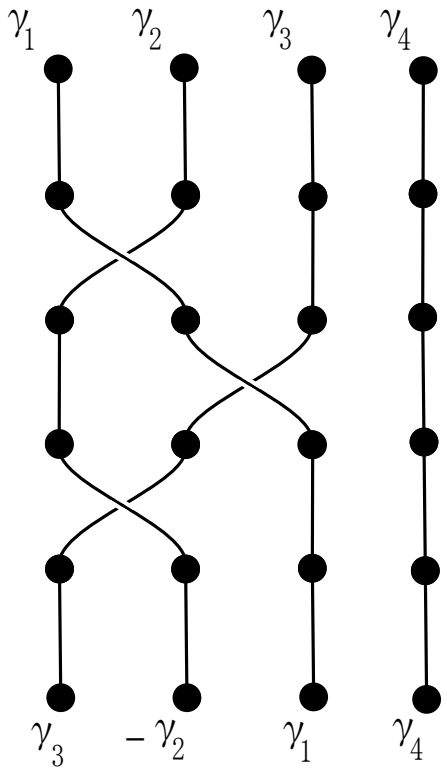

Figure 4.7: Hadamard gate braid in the braiding diagram formalism.

The effect on the number states:

$$\begin{aligned} \hat{U}_{12}\hat{U}_{23}\hat{U}_{12}\,|\hat{0}\rangle &= ... = \frac{1}{\sqrt{2}}(\gamma_1\gamma_2 + \gamma_2\gamma_3)\,|\hat{0}\rangle = ... = \frac{i}{\sqrt{2}}(|\hat{0}\rangle + |\hat{1}\rangle), \\ \hat{U}_{12}\hat{U}_{23}\hat{U}_{12}\,|\hat{1}\rangle &= ... = \frac{1}{\sqrt{2}}(\gamma_1\gamma_2 + \gamma_2\gamma_3)\,|\hat{1}\rangle = ... = \frac{i}{\sqrt{2}}(|\hat{0}\rangle - |\hat{1}\rangle). \end{aligned} \tag{4.16}$$

This verifies that the transformation on $|\hat{0}\rangle$ and $|\hat{1}\rangle$ form the expected superposition state, up to a phase. See appendix eqs. (A.2, A.3, A.4 and A.5) for details.

4.2.3 Universal Gates

The two single-qubit gates discussed above, the Pauli X-gate and the Hadamard gate, were explicitly constructed by braiding operations in the T-junction network in order to present a first step to implement quantum gates. This may be a first step on the way towards potentially using the nanowire network for universal quantum computing. The two-qubit gate CNOT requires additional Majorana modes to be braided, beyond what was needed for the Pauli X- and Hadamard gates. Additional measurement capabilities need to be added to the nanowire network in order for the $\pi/8$ phase gate to be implemented [31].

5

Discussion

5.1 Experimental Outlook

Many of the required experimental feats required to experimentally test the T-junction design have already been demonstrated. These include patterning of multiple gates on the micron scale [33] and generating proximity-induced superconductivity in an InAs wire [34].

Another potential step forward is suggested by the numerical study of Majorana braiding dynamics. Simulations performed by Amorim et al. [35] suggest that the time scale necessary to braid Majorana modes around each other is at the order of a few nanoseconds or in the GHz realm of electrical components. In fact, the experimental realization of a T-junction is expected to be within reach in the next few years [36].

A challenge to the interpretations of the experiments done in order to demonstrate Majorana zero modes in nanowires have come in the form of competing explanations: Andreev bound states of near zero-energy in the topologically trivial phase rather well reproduce the phenomenology of charge transport which originally was believed to be a "smoking gun" of Majorana modes, cf. [37],[38] and [39]. A recent proposal by Avila et al. [40] suggests however that some of the Andreev bound states in fact shares all the properties of Majorana modes and that the distinction between the two disappears.

The research on Majorana zero modes continues to provide new and interesting challenges both for the experimental as well as for the theoretical side of condensed matter physics.

5.2 Conclusions

We have studied the nanowire construction proposed by Alicea et.al [1] and have used the T-junction formalism to explicitly create two quantum gates, the **NOT (Pauli X)** gate and the **Hadamard** gate. These two gates are in themselves components used in order to create larger qubit gates and as such they can be seen as building block to be used in the future. In this thesis, elementary braiding operations of Majorana modes have been translated into the corresponding series of transports required to implement quantum gates in an experimental system. As such it provides a first guide to bridging the mathematical operations and practical implementations.

Bibliography

[1] J. Alicea, Y. Oreg, G. Refael, F. von Oppen, M. P. A. Fisher, Non-abelian statistics and topological quantum information processing in 1d wire networks, Nature Physics 7 (5) (2011) 412–417.
URL http://dx.doi.org/10.1038/nphys1915

[2] E. Majorana, L. Maiani, A symmetric theory of electrons and positrons, [Springer Berlin Heidelberg, Berlin, Heidelberg, 2006], Ch. 9, pp. 201–233.
URL https://doi.org/10.1007/978-3-540-48095-2_10

[3] J. Alicea, New directions in the pursuit of Majorana fermions in solid state systems, Reports on Progress in Physics 75 (7) (2012) 076501.

[4] C. Nayak, S. H. Simon, A. Stern, M. Freedman, S. Das Sarma, Non-Abelian anyons and topological quantum computation, Reviews of Modern Physics 80 (2008) 1083–1159.

[5] S. Hannestad, Neutrino physics and precision cosmology, ArXiv:1605.03829[hep-ph].
URL https://arxiv.org/abs/1605.03829

[6] K. N. Abazajian, Et.al, Light Sterile Neutrinos: A White Paper, ArXiv:1204.5379[hep-ph].
URL https://arxiv.org/abs/1204.5379

[7] P. A. M. Dirac, The quantum theory of the electron, Proceedings of the Royal Society of London A: Mathematical, Physical and Engineering Sciences 117 (778) (1928) 610–624.
URL http://rspa.royalsocietypublishing.org/content/117/778/610

[8] D. Griffiths, Quantum Electrodynamics, WILEY-VCH Verlag GmbH & Co., 2017, Ch. 7, pp. 225–229.
URL http://eu.wiley.com/WileyCDA/WileyTitle/productCd-3527406018,subjectCd-PH20.html

[9] C. D. Anderson, The positive electron, Physical Review 43 (1933) 491–494.
URL https://link.aps.org/doi/10.1103/PhysRev.43.491

[10] L. Alvarez-Gaume, M. A. Vazquez-Mozo, Introductory Lectures on Quantum Field Theory, arXiv:hep-th/0510040.

[11] P. B. Pal, Dirac, Majorana, and Weyl fermions, American Journal of Physics 79 (2011) 485–498.
URL https://arxiv.org/pdf/1006.1718.pdf

[12] R. Clyde, L Cowan Frederick, The Neutrino, Nature 178 (1956) 446–449.
URL http://dx.doi.org/10.1038/178446a0

[13] A. B. Balantekin, W. C. Haxton, Neutrino oscillations, Progress in Particle and Nuclear Physics 71 (2013) 150–161.

[14] F. Wilczek, Majorana returns, Nature Physics 5 (9) (2009) 614–618.
URL http://dx.doi.org/10.1038/nphys1380

[15] J. Bardeen, L. N. Cooper, J. R. Schrieffer, Theory of superconductivity, Physical Review 108 (1957) 1175–1204.
URL https://link.aps.org/doi/10.1103/PhysRev.108.1175

[16] N. Ashcroft, N. Mermin, Solid State Physics, Cengage Learning, 1976.
URL https://books.google.se/books?id=x_s_YAAACAAJ

[17] "Second quantization" (the occupation-number representation), http://physics.gu.se/~tfkhj/OsloSecondQuant.pdf.

[18] Fermi surface example, https://nptel.ac.in/courses/113106040/Lecture25.pdf.

[19] Fermi many-body example, http://fy.chalmers.se/~hellsing/Many_Body-Physics/kap4pres.pdf.

[20] W. Y. Liang, Excitons, Physics Education 5 (4) (1970) 226.
URL http://stacks.iop.org/0031-9120/5/i=4/a=003

[21] R. M. Lutchyn, J. D. Sau, S. Das Sarma, Majorana Fermions and a Topological Phase Transition in Semiconductor-Superconductor Heterostructures, Physical Review Letters 105 (7) (2010) 077001.

[22] Y. Oreg, G. Refael, F. von Oppen, Helical liquids and majorana bound states in quantum wires, Physical Review Letters 105 (2010) 177002.
URL https://link.aps.org/doi/10.1103/PhysRevLett.105.177002

[23] M. Leijnse, K. Flensberg, Introduction to topological superconductivity and majorana fermions, Semiconductor Science and Technology 27 (12) (2012) 124003.
URL http://stacks.iop.org/0268-1242/27/i=12/a=124003

[24] D. A. Ivanov, Non-abelian statistics of half-quantum vortices in p-wave superconductors, Physical Review Letters 86 (2001) 268–271.
URL https://link.aps.org/doi/10.1103/PhysRevLett.86.268

[25] Spherical Harmonic list, http://mathworld.wolfram.com/SphericalHarmonic.html.

[26] A. Y. Kitaev, Unpaired Majorana fermions in quantum wires, Physics Uspekhi 44 (2001) 131.

[27] A. Steane, Quantum computing, Reports on Progress in Physics 61 (1998) 117–173.

[28] A. Ekert, P. M. Hayden, H. Inamori, Basic Concepts in Quantum Computation, in: R. Kaiser, C. Westbrook, F. David (Eds.), Coherent Atomic Matter Waves, Vol. 72, 2001, p. 661.

[29] D. Deutsch, Quantum theory, the Church–Turing principle and the universal quantum computer, Proceedings of the Royal Society of London, A, 1985 400:97.

[30] CNOT Gate Example, `https://quantiki.org/wiki/CNOT`.

[31] S. D. Sarma, M. Freedman, C. Nayak, Majorana zero modes and topological quantum computation, npj Quantum Information 1 (2015) 15001.

[32] L. Fu, C. L. Kane, Superconducting proximity effect and majorana fermions at the surface of a topological insulator, Physical Review Letters 100 (2008) 096407.
URL `https://link.aps.org/doi/10.1103/PhysRevLett.100.096407`

[33] H. Steinberg, O. M. Auslaender, A. Yacoby, J. Qian, G. A. Fiete, Y. Tserkovnyak, B. I. Halperin, K. W. Baldwin, L. N. Pfeiffer, K. W. West, Localization transition in a ballistic quantum wire, Physical Review B 73 (2006) 113307.
URL `https://link.aps.org/doi/10.1103/PhysRevB.73.113307`

[34] Y. Doh, J. van Dam, A. Roest, E. Bakkers, L. Kouwenhoven, S. De Franceschi, Tunable supercurrent through semiconductor nanowires, Science 309 (2005) 272–275.

[35] C. S. Amorim, K. Ebihara, A. Yamakage, Y. Tanaka, M. Sato, Majorana braiding dynamics in nanowires, Physical Review B 91 (2015) 174305.
URL `https://link.aps.org/doi/10.1103/PhysRevB.91.174305`

[36] M. T. Deng, S. Vaitiekėnas, E. B. Hansen, J. Danon, M. Leijnse, K. Flensberg, J. Nygård, P. Krogstrup, C. M. Marcus, Majorana bound state in a coupled quantum-dot hybrid-nanowire system, Science 354 (2016) 1557–1562.

[37] C.-X. Liu, J. D. Sau, S. Das Sarma, Role of dissipation in realistic majorana nanowires, Physical Review B 95 (2017) 054502.
URL `https://link.aps.org/doi/10.1103/PhysRevB.95.054502`

[38] C. Moore, T. D. Stanescu, S. Tewari, Two-terminal charge tunneling: Disentangling majorana zero modes from partially separated andreev bound states in semiconductor-superconductor heterostructures, Physical Review B 97 (2018) 165302.
URL `https://link.aps.org/doi/10.1103/PhysRevB.97.165302`

[39] A. Vuik, B. Nijholt, A. R. Akhmerov, M. Wimmer, Reproducing topological properties with quasi-Majorana states, ArXiv e-prints.

[40] J. Avila, F. Peñaranda, E. Prada, P. San-Jose, R. Aguado, Non-Hermitian topology: a unifying framework for the Andreev versus Majorana states controversy, ArXiv e-prints.

A

Equations

A.1 Full Derivation of Eq. (2.73)

$$
\begin{aligned}
H = & -t \sum_{x=1}^{N-1} \left[c_x^\dagger c_{x+1} + c_{x+1}^\dagger c_x + e^{i\phi} c_x c_{x+1} + e^{-i\phi} c_{x+1}^\dagger c_x^\dagger \right] \\
= & \frac{-t}{4} \sum_{x=1}^{N-1} \Big[(\gamma_{2x} - i\gamma_{2x-1})(\gamma_{2(x+1)} + i\gamma_{2(x+1)-1}) + (\gamma_{2(x+1)} - i\gamma_{2(x+1)-1})(\gamma_{2x} + i\gamma_{2x-1}) \\
& \qquad + (\gamma_{2x} + i\gamma_{2x-1})(\gamma_{2(x+1)} + i\gamma_{2(x+1)-1}) + (\gamma_{2(x+1)} - i\gamma_{2(x+1)-1})(\gamma_{2x} - i\gamma_{2x-1}) \Big] \\
= & \frac{-t}{4} \sum_{x=1}^{N-1} \Big[(\gamma_{2x}\gamma_{2(x+1)-1} + i\gamma_{2x}\gamma_{2(x+1)-1} - i\gamma_{2x-1}\gamma_{2(x+1)} - i^2\gamma_{2x-1}\gamma_{2(x+1)-1}) \\
& \qquad + (\gamma_{2(x+1)}\gamma_{2x} + i\gamma_{2(x+1)}\gamma_{2x-1} - i\gamma_{2(x+1)-1}\gamma_{2x} - i^2\gamma_{2(x+1)-1}\gamma_{2x-1}) \\
& \qquad + (\gamma_{2x}\gamma_{2(x+1)} + i\gamma_{2x}\gamma_{2(x+1)-1} + i\gamma_{2x-1}\gamma_{2(x+1)} + i^2\gamma_{2x-1}\gamma_{2(x+1)-1}) \\
& \qquad + (\gamma_{2(x+1)}\gamma_{2x} - i\gamma_{2(x+1)}\gamma_{2x-1} - i\gamma_{2(x+1)-1\gamma_{2x}} + i^2\gamma_{2(x+1)-1}\gamma_{2x-1}) \Big] \\
= & -it \sum_{x=1}^{N-1} \gamma_{2x}\gamma_{2(x+1)-1}.
\end{aligned}
\tag{A.1}
$$

A.2 Majoranas $\gamma_1\gamma_2$ Acting on Number State $|0\rangle$

$$\begin{aligned}
\gamma_1\gamma_2 |0\rangle &= \gamma_1\gamma_2 f_1 |1\rangle \\
&= \gamma_1\gamma_2 \frac{1}{2}(\gamma_1 + i\gamma_2)|1\rangle \\
&= \frac{1}{2}(\gamma_1\gamma_2\gamma_1 + i\gamma_1\gamma_2\gamma_2)|1\rangle \\
&= \frac{1}{2}(-\gamma_2 + i\gamma_1)|1\rangle \\
&= \frac{i}{2}(\gamma_1 + i\gamma_2)|1\rangle \\
&= i f_1 |1\rangle \\
&= i|0\rangle ,
\end{aligned} \tag{A.2}$$

A.3 Majorana Modes $\gamma_1\gamma_2$ Acting on Number State $|1\rangle$

$$\begin{aligned}
\gamma_1\gamma_2 |1\rangle &= \gamma_1\gamma_2 f_1^\dagger |0\rangle \\
&= \gamma_1\gamma_2 \frac{1}{2}(\gamma_1 - i\gamma_2)|0\rangle \\
&= \frac{1}{2}(\gamma_1\gamma_2\gamma_1 - i\gamma_1\gamma_2\gamma_2)|0\rangle \\
&= \frac{1}{2}(-\gamma_2 - i\gamma_1)|0\rangle \\
&= \frac{-i}{2}(\gamma_1 - i\gamma_2)|0\rangle \\
&= -i f_1^\dagger |0\rangle \\
&= -i|1\rangle ,
\end{aligned} \tag{A.3}$$

$$\gamma_1\gamma_2 \mathrel{\widehat{=}} \begin{bmatrix} i & 0 \\ 0 & -i \end{bmatrix},$$

$$-i\gamma_1\gamma_2 = \sigma_z.$$

A.4 Majorana Modes $\gamma_2\gamma_3$ Acting on Qubit $|\hat{0}\rangle$

$$\begin{aligned}
\gamma_2\gamma_3\,|\hat{0}\rangle &= \gamma_2\gamma_3\; f_2\, f_1\,|\hat{1}\rangle \\
&= \gamma_2\gamma_3 \frac{1}{4}\left([\gamma_3 + i\gamma_4]\,[\gamma_1 + i\gamma_2]\right)|\hat{1}\rangle \\
&= \frac{1}{4}\left([\gamma_2\gamma_3\gamma_3 + i\gamma_2\gamma_3\gamma_4]\,[\gamma_1 + i\gamma_2]\right)|\hat{1}\rangle \\
&= \frac{1}{4}\left(\gamma_2\gamma_1 + i\gamma_2\gamma_3\gamma_4\gamma_1 + i\gamma_2\gamma_2 - \gamma_2\gamma_3\gamma_4\gamma_2\right)|\hat{1}\rangle \\
&= \frac{1}{4}\left(-\gamma_1\gamma_2 - i\gamma_1\gamma_2\gamma_3\gamma_4 + i - \gamma_3\gamma_4\right)|\hat{1}\rangle \\
&= \frac{1}{4}\Big(-\gamma_1\gamma_2\,|\hat{1}\rangle - i\gamma_1\gamma_2\gamma_3\gamma_4\,|\hat{1}\rangle + i\,|\hat{1}\rangle - \gamma_3\gamma_4\,|\hat{1}\rangle\Big) \\
&= \frac{1}{4}\Big(-(-i)\,|\hat{1}\rangle - i\gamma_1\gamma_2(-i)\,|\hat{1}\rangle + i\,|\hat{1}\rangle - (-i)\,|\hat{1}\rangle\Big) \\
&= \frac{1}{4}\Big(i\,|\hat{1}\rangle - i(-1)\,|\hat{1}\rangle + i\,|\hat{1}\rangle + i\,|\hat{1}\rangle\Big) \\
&= \frac{1}{4}\left(i + i + i + i\right)|\hat{1}\rangle \\
&= i\,|\hat{1}\rangle\,,
\end{aligned} \tag{A.4}$$

A.5 Majorana Modes $\gamma_2\gamma_3$ Acting on Qubit $|\hat{1}\rangle$

$$\begin{aligned}
\gamma_2\gamma_3\,|\hat{1}\rangle &= \gamma_2\gamma_3\; f_1^\dagger\, f_2^\dagger\,|\hat{0}\rangle \\
&= \gamma_2\gamma_3 \frac{1}{4}\left([\gamma_1 - i\gamma_2]\,[\gamma_3 - i\gamma_4]\right)|\hat{0}\rangle \\
&= \frac{1}{4}\left([\gamma_2\gamma_3\gamma_1 - i\gamma_2\gamma_3\gamma_2]\,[\gamma_3 - i\gamma_4]\right)|\hat{0}\rangle \\
&= \frac{1}{4}\left(\gamma_2\gamma_3\gamma_1\gamma_3 - i\gamma_2\gamma_3\gamma_1\gamma_4 - i\gamma_2\gamma_3\gamma_2\gamma_3 - \gamma_2\gamma_3\gamma_2\gamma_4\right)|\hat{0}\rangle \\
&= \frac{1}{4}\left(\gamma_1\gamma_2 - i\gamma_1\gamma_2\gamma_3\gamma_4 + i + \gamma_3\gamma_4\right)|\hat{0}\rangle \\
&= \frac{1}{4}\Big(i\,|\hat{0}\rangle\; - i(i)(i)\,|\hat{0}\rangle\; + i\,|\hat{0}\rangle\; + i\,|\hat{0}\rangle\Big) \\
&= \frac{1}{4}\left(i + i + i + i\right)|\hat{0}\rangle \\
&= i\,|\hat{0}\rangle\,,
\end{aligned} \tag{A.5}$$

$$\gamma_2\gamma_3 \mathrel{\widehat{=}} \begin{bmatrix} 0 & i \\ i & 0 \end{bmatrix},$$

$$-i\gamma_2\gamma_3 = \sigma_x.$$

A.6 Majorana Modes $\gamma_1\gamma_4$ Acting on Qubit $|\hat{0}\rangle$

$$\begin{aligned}\gamma_1\gamma_4\,|\hat{0}\rangle &= \gamma_1\gamma_4\, f_2 f_1\,|\hat{1}\rangle \\ &= \gamma_1\gamma_4 \frac{1}{4}\left([\gamma_3 + i\gamma_4][\gamma_1 + i\gamma_2]\right)|\hat{1}\rangle \\ &= \frac{1}{4}([\gamma_1\gamma_4\gamma_3 + i\gamma_1][\gamma_1 + i\gamma_2])\,|\hat{1}\rangle \\ &= \frac{1}{4}(i - \gamma_1\gamma_2 - \gamma_3\gamma_4 - i\gamma_1\gamma_2\gamma_3\gamma_4)\,|\hat{1}\rangle \\ &= i\,|\hat{1}\rangle\,,\end{aligned} \tag{A.6}$$

A.7 Majorana Modes $\gamma_1\gamma_4$ Acting on Qubit $|\hat{1}\rangle$

$$\begin{aligned}\gamma_1\gamma_4\,|\hat{1}\rangle &= \gamma_1\gamma_4\, f_1^\dagger f_2^\dagger\,|\hat{0}\rangle \\ &= \gamma_1\gamma_4 \frac{1}{4}\left([\gamma_1 - i\gamma_2][\gamma_3 - i\gamma_4]\right)|\hat{0}\rangle \\ &= \frac{1}{4}([-\gamma_4 - i\gamma_1\gamma_4\gamma_2][\gamma_3 - i\gamma_4])\,|\hat{0}\rangle \\ &= \frac{1}{4}(i + \gamma_1\gamma_2 + \gamma_3\gamma_4 - i\gamma_1\gamma_2\gamma_3\gamma_4)\,|\hat{0}\rangle \\ &= i\,|\hat{0}\rangle\,,\end{aligned} \tag{A.7}$$

$$\gamma_1\gamma_4 \mathrel{\widehat{=}} \begin{bmatrix} 0 & i \\ i & 0 \end{bmatrix},$$

$$-i\gamma_1\gamma_4 = \sigma_x.$$

A.8 Majorana Modes $\gamma_1\gamma_3$ Acting on Qubit $|\hat{0}\rangle$

$$\begin{aligned}
\gamma_1\gamma_3\,|\hat{0}\rangle &= \gamma_1\gamma_3\; f_2 f_1\,|\hat{1}\rangle \\
&= \gamma_1\gamma_3 \frac{1}{4}\left([\gamma_3 + i\gamma_4]\,[\gamma_1 + i\gamma_2]\right)|\hat{1}\rangle \\
&= \frac{1}{4}\left([\gamma_1 + i\gamma_1\gamma_3\gamma_4][\gamma_1 + i\gamma_2]\right)|\hat{1}\rangle \\
&= \frac{1}{4}\left(1 + i\gamma_1\gamma_2 + i\gamma_1\gamma_3\gamma_4\gamma_1 - \gamma_1\gamma_3\gamma_4\gamma_2\right)|\hat{1}\rangle \\
&= \frac{1}{4}\left(1 + i\gamma_1\gamma_2 + i\gamma_3\gamma_4 - \gamma_1\gamma_2\gamma_3\gamma_4\right)|\hat{1}\rangle \\
&= \frac{1}{4}\Big(|\hat{1}\rangle + i(-i)\,|\hat{1}\rangle + i(-i)\,|\hat{1}\rangle - (-i)(-i)\,|\hat{1}\rangle\Big) \\
&= \frac{1}{4}\left(1 + 1 + 1 + 1\right)|\hat{1}\rangle \\
&= |\hat{1}\rangle\,,
\end{aligned} \tag{A.8}$$

A.9 Majorana Modes $\gamma_1\gamma_3$ Acting on Qubit $|\hat{1}\rangle$

$$\begin{aligned}
\gamma_1\gamma_3\,|\hat{1}\rangle &= \gamma_1\gamma_3\; f_1^\dagger f_2^\dagger\,|\hat{0}\rangle \\
&= \gamma_1\gamma_3 \frac{1}{4}\left([\gamma_1 - i\gamma_2]\,[\gamma_3 - i\gamma_4]\right)|\hat{0}\rangle \\
&= \frac{1}{4}\left([\gamma_1\gamma_3\gamma_1 - i\gamma_1\gamma_3\gamma_2]\,[\gamma_3 - i\gamma_4]\right)|\hat{0}\rangle \\
&= \frac{1}{4}\left(-\gamma_3 + i\gamma_1\gamma_2\gamma_3]\,[\gamma_3 - i\gamma_4]\right)|\hat{0}\rangle \\
&= \frac{1}{4}\left(-\gamma_3\gamma_3 + i\gamma_3\gamma_4 + i\gamma_1\gamma_2 + \gamma_1\gamma_2\gamma_3\gamma_4\right)|\hat{0}\rangle \\
&= \frac{1}{4}\left(-1 + i(i) + i(i) + (i)(i)\right)|\hat{0}\rangle \\
&= -1\,|\hat{0}\rangle\,,
\end{aligned} \tag{A.9}$$

$$\gamma_1\gamma_3 \mathrel{\widehat{=}} \begin{bmatrix} 0 & -1 \\ 1 & 0 \end{bmatrix},$$

$$i\gamma_1\gamma_3 = \sigma_y.$$

A.10 Majorana Modes $\gamma_2\gamma_4$ Acting on Qubit $|\hat{0}\rangle$

$$\begin{aligned}
\gamma_2\gamma_4\,|\hat{0}\rangle &= \gamma_2\gamma_4\, f_2 f_1\,|\hat{1}\rangle \\
&= \gamma_2\gamma_4 \frac{1}{4}\left([\gamma_3 + i\gamma_4][\gamma_1 + i\gamma_2]\right)|\hat{1}\rangle \\
&= \frac{1}{4}\left(\gamma_2\gamma_4\gamma_3\gamma_1 + i\gamma_2\gamma_4\gamma_3\gamma_2 + i\gamma_2\gamma_4\gamma_4\gamma_1 - \gamma_2\gamma_4\gamma_4\gamma_2\right)|\hat{1}\rangle \\
&= \frac{1}{4}\left(\gamma_1\gamma_2\gamma_3\gamma_4 - i\gamma_3\gamma_4 - i\gamma_1\gamma_2 - 1\right)|\hat{1}\rangle \\
&= \frac{1}{4}\left((-i)(-i) - i(-i) - i(-i) - 1\right)|\hat{1}\rangle \\
&= \frac{1}{4}\left(-1 - 1 - 1 - 1\right)|\hat{1}\rangle \\
&= -\,|\hat{1}\rangle\,,
\end{aligned} \tag{A.10}$$

A.11 Majorana Modes $\gamma_2\gamma_4$ Acting on Qubit $|\hat{1}\rangle$

$$\begin{aligned}
\gamma_2\gamma_4\,|\hat{1}\rangle &= \gamma_2\gamma_4\, f_1^\dagger f_2^\dagger\,|\hat{0}\rangle \\
&= \gamma_2\gamma_4 \frac{1}{4}\left([\gamma_1 - i\gamma_2][\gamma_3 - i\gamma_4]\right)|\hat{0}\rangle = ... \\
&= \frac{1}{4}\left(-\gamma_1\gamma_2\gamma_3\gamma_4 - i\gamma_1\gamma_2 - i\gamma_3\gamma_4 + 1\right)|\hat{0}\rangle \\
&= \frac{1}{4}\left(1 + 1 + 1 + 1\right)|\hat{0}\rangle \\
&= |\hat{0}\rangle\,,
\end{aligned} \tag{A.11}$$

$$\gamma_2\gamma_4 \mathrel{\widehat{=}} \begin{bmatrix} 0 & 1 \\ -1 & 0 \end{bmatrix},$$

$$-i\gamma_2\gamma_4 = \sigma_y.$$

A.12 Majorana Modes in eq. (3.28)

Expanded derivation of eq. (3.28) from eq. (3.27):

$$\begin{aligned} H(\lambda_a) = -\mu \sum_{y=1}^{N} c_y^\dagger c_y + \sum_{x=1}^{2N} t \left(e^{-i\frac{\phi_x}{2}} c_x^\dagger + e^{i\frac{\phi_x}{2}} c_x \right) \left(e^{-i\frac{\phi_x}{2}} c_{x+1}^\dagger - e^{i\frac{\phi_x}{2}} c_{x+1} \right) \\ \phi_x = \phi + \pi \quad \text{for } x \leq N, \\ \phi_x = \phi \qquad \text{for } x \geq N+1. \end{aligned} \tag{A.12}$$

If we look at the $x = 1$ case, the leftmost atomic orbital in the wire, we have that

$$\begin{aligned} & t \left(e^{-i\frac{\phi+\pi}{2}} c_1^\dagger + e^{i\frac{\phi+\pi}{2}} c_1 \right) \left(e^{-i\frac{\phi+\pi}{2}} c_2^\dagger - e^{i\frac{\phi+\pi}{2}} c_2 \right) \\ = & \, t \left(e^{-i\phi+\pi} c_1^\dagger c_2^\dagger - c_1^\dagger c_2 + c_1 c_2^\dagger - e^{i\phi+\pi} c_1 c_2 \right). \end{aligned} \tag{A.13}$$

We see that no $\left(e^{-i\frac{\phi+\pi}{2}}\right) c_1^\dagger + \left(e^{i\frac{\phi+\pi}{2}}\right) c_1$ combination exists in the Hamiltonian. A similar derivation shows that the $e^{\left(-i\frac{\phi}{2}\right)} c_{(2N+1)}^\dagger + e^{\left(i\frac{\phi}{2}\right)} c_{(2N+1)}$ combination also does not appear.

A.13 Operator U_{12} Acting on the Qubit $|\hat{0}\rangle$

$$\begin{aligned} U_{12} |\hat{0}\rangle = & \, \frac{1}{\sqrt{2}} (1 - \gamma_1\gamma_2) \, \frac{1}{4} (\gamma_3 + i\gamma_4)(\gamma_1 + i\gamma_2) |\hat{1}\rangle \\ = & \, \frac{1}{\sqrt{2}\,4} (\gamma_3\gamma_1 + i\gamma_3\gamma_2 + i\gamma_4\gamma_1 - \gamma_4\gamma_2 - \gamma_1\gamma_2\gamma_3\gamma_1 \\ & \quad - i\gamma_1\gamma_2\gamma_3\gamma_2 - i\gamma_1\gamma_2\gamma_4\gamma_1 + \gamma_1\gamma_2\gamma_4\gamma_2) |\hat{1}\rangle \\ = & \, \frac{1}{\sqrt{2}\,4} \left[(-1+i)\gamma_1\gamma_3 - (1+i)\gamma_1\gamma_4 - (1+i)\gamma_2\gamma_3 + (1-i)\gamma_2\gamma_4 \right] |\hat{1}\rangle \\ = & \, \frac{1}{\sqrt{2}\,4} \left[(-1+i)(-1) - (1+i)(i) - (1+i)(i) + (1-i)(1) \right] |\hat{0}\rangle \\ = & \, \frac{1}{\sqrt{2}} (1-i) |\hat{0}\rangle . \end{aligned} \tag{A.14}$$

A.14 Operator U_{23} Acting on Qubit $|\hat{0}\rangle$

$$\begin{aligned}
U_{23}|\hat{0}\rangle &= \frac{1}{\sqrt{2}}(1-\gamma_1\gamma_2)\,\frac{1}{4}(\gamma_3+i\gamma_4)(\gamma_1+i\gamma_2)\,|\hat{1}\rangle \\
&= \frac{1}{\sqrt{2}\,4}(\gamma_3\gamma_1 + i\gamma_3\gamma_2 + i\gamma_4\gamma_1 - \gamma_4\gamma_2 - \gamma_2\gamma_3\gamma_3\gamma_1 \\
&\qquad -i\gamma_2\gamma_3\gamma_3\gamma_2 - i\gamma_2\gamma_3\gamma_4\gamma_1 + \gamma_2\gamma_3\gamma_4\gamma_2)\,|\hat{1}\rangle \\
&= \frac{1}{\sqrt{2}\,4}(-\gamma_1\gamma_3 - i\gamma_2\gamma_3 - i\gamma_1\gamma_4 + \gamma_2\gamma_4 + \gamma_1\gamma_2 \\
&\qquad -i + i\gamma_1\gamma_2\gamma_3\gamma_4 + \gamma_3\gamma_4)\,|\hat{1}\rangle \\
&= \frac{1}{\sqrt{2}\,4}\Big(|\hat{0}\rangle + |\hat{0}\rangle + |\hat{0}\rangle + |\hat{0}\rangle + (-i-i-i-i)\,|\hat{1}\rangle\Big) \\
&= \frac{1}{\sqrt{2}}\Big(|\hat{0}\rangle - i\,|\hat{1}\rangle\Big).
\end{aligned} \tag{A.15}$$

A.15 Operator U_{23} Acting on Qubit $|\hat{1}\rangle$

The result of acting with braid operator U_{23} on a qubit state

$$\begin{aligned}
U_{23}|\hat{1}\rangle &= \frac{1}{\sqrt{2}}(1-\gamma_2\gamma_3)\,\frac{1}{4}(\gamma_1-i\gamma_2)(\gamma_3-i\gamma_4)\,|\hat{0}\rangle \\
&= \frac{1}{\sqrt{2}\,4}(\gamma_1\gamma_3 - i\gamma_1\gamma_4 - i\gamma_2\gamma_3 - \gamma_2\gamma_4 - \gamma_2\gamma_3\gamma_1\gamma_3 \\
&\qquad +i\gamma_2\gamma_3\gamma_1\gamma_4 + i\gamma_2\gamma_3\gamma_2\gamma_3 + \gamma_2\gamma_3\gamma_2\gamma_4)\,|\hat{0}\rangle \\
&= \frac{1}{\sqrt{2}\,4}(\gamma_1\gamma_3 - i\gamma_1\gamma_4 - i\gamma_2\gamma_3 - \gamma_2\gamma_4 - \gamma_1\gamma_2 \\
&\qquad +i\gamma_1\gamma_2\gamma_3\gamma_4 - i - \gamma_3\gamma_4)\,|\hat{0}\rangle \\
&= \frac{1}{\sqrt{2}\,4}\Big(|\hat{1}\rangle + |\hat{1}\rangle + |\hat{1}\rangle + |\hat{1}\rangle + (-i-i-i-i)\,|\hat{0}\rangle\Big) \\
&= \frac{1}{\sqrt{2}}\Big(-i\,|\hat{0}\rangle + |\hat{1}\rangle\Big).
\end{aligned} \tag{A.16}$$

A.16 Braid Operator U_{23} Squared

$$\begin{aligned}
U_{23}^2 &= \frac{1}{2}(1-\gamma_2\gamma_3)(1-\gamma_2\gamma_3) = \frac{1}{2}(1-2\gamma_2\gamma_3+\gamma_2\gamma_3\gamma_2\gamma_3) = -\gamma_2\gamma_3, \\
\hat{U}_{23}^2 &= \frac{1}{2}(1+\gamma_2\gamma_3)(1+\gamma_2\gamma_3) = \frac{1}{2}(1+2\gamma_2\gamma_3+\gamma_2\gamma_3\gamma_2\gamma_3) = \gamma_2\gamma_3.
\end{aligned} \tag{A.17}$$